How to Unlock Time Series Editing?
A Diffusion-Driven Approach with Multi-Grained Control

Hao Yu[1] Chu Xin Cheng[2] Runlong Yu[3] Yuyang Ye[4] Shiwei Tong[5] Zhaofeng Liu[5] Defu Lian[6]

Abstract

Recent advances in time series generation have shown promise, yet controlling properties in generated sequences remains challenging. Time Series Editing (TSE)—making precise modifications while preserving temporal coherence—consider both point-level constraints and segment-level controls that current methods struggle to provide. We introduce the CocktailEdit framework to enable simultaneous, flexible control across different types of constraints. This framework combines two key mechanisms: a confidence-weighted anchor control for point-wise constraints and a classifier-based control for managing statistical properties such as sums and averages over segments. Our methods achieve precise local control during the denoising inference stage while maintaining temporal coherence and integrating seamlessly, with any conditionally trained diffusion-based time series models. Extensive experiments across diverse datasets and models demonstrate its effectiveness. Our work bridges the gap between pure generative modeling and real-world time series editing needs, offering a flexible solution for human-in-the-loop time series generation and editing.

The code[1] and demo[2] are provided for validation.

1. Introduction

Time series data is highly prevalent in our daily lives, from financial markets to healthcare systems, where time series generation (TSG) is increasingly vital for analysis and prediction (Wang et al., 2024). Current approaches excel in unconditionally generating time series data, such as VAEs (Lee et al., 2023; Bao et al., 2024; Sommers et al., 2024), GANs (Goodfellow, 2016; Wiese et al., 2020; Miao et al., 2021), and diffusion models (Kong et al., 2020; Rasul et al., 2021; Li et al., 2022; Alcaraz & Strodthoff, 2022). However, this unconditionally generated time series may be impractical in many applications. For example, in the retail industry, companies hope to forecast the revenue of an unreleased product. Unconditionally generated data may fail to satisfy desired properties that seem obvious to producers, i.e. sales should peak during holiday seasons or after coupons mailed. Therefore, we hope to guide the generation process with certain prior knowledge. A simple case of prior knowledge would be data points that the generated curve must pass through. In such case, an intuitive method would be to manually replace the point on the generated curve. However, this method does not consider the possibility that the point could be correlated with the rest of the time series curve. Therefore, this post-editing method risks generating out-of-distribution time series and does not leverage any information provided to us from partially observed data points or known trends. Thus, we hope to develop a principled way for generating time series while obeying certain user-specified rules, i.e. achieving controlled TSG.

We developed CocktailEdit, a unifying framework named for its ability to mix and blend different types of controls—much like mixing ingredients in a cocktail—to create precisely tailored time series outputs. Our framework embodies a wide range of various control types illustrated in Figure 1. We categorize these controls by their range of focus. For example, we may have user-provided point-wise control, such as a single measurement on a fixed date with its confidence interval. On the other hand, we can also focus on global properties such as overall trend, periodicity, or specific data statistics (average, sum, optimizers, etc.). We regard these problems as an overall Time Series Editing (TSE) challenge (Jing et al., 2024), tackling this challenge means producing time series data that can simultaneously satisfy user-defined constraints while maintaining temporal coherence and distributional fidelity.

[1]Department of Computer Science, McGill University, Canada [2]California Institute of Technology, United States [3]University of Pittsburgh, United States [4]Rutgers University, United States [5]IEGG, Tencent, China [6]University of Science and Technology of China, China. Correspondence to: Hao Yu <hao.yu2@mail.mcgill.ca>, Shiwei Tong <shiweitong@tencent.com>.

[1] Code are available here: Anonymous Git Repository

[2] Time Series Editor are available here: Huggingface Space

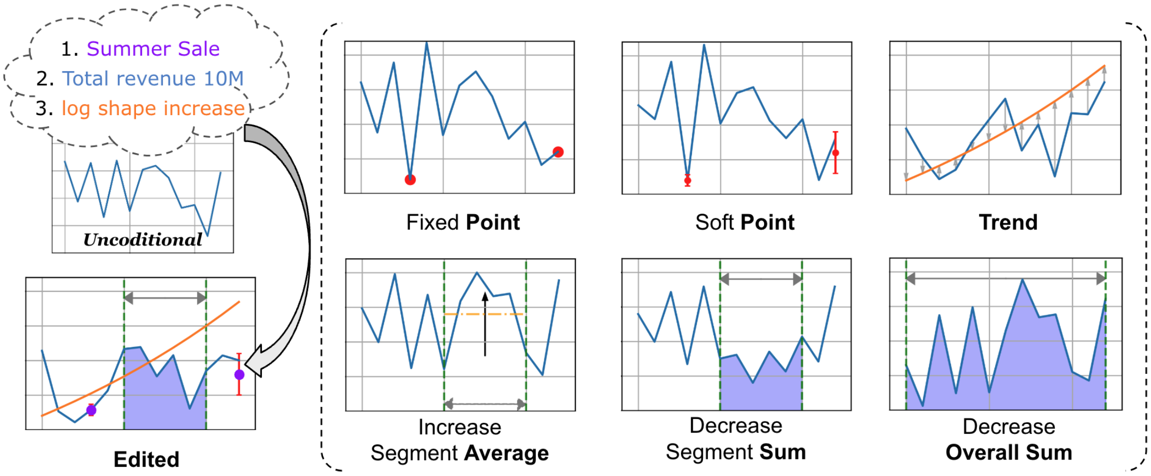

Figure 1. Overview of Time Series Editing (TSE): From unconditional generation to Time Series Editing, including (a) Point-level control using fixed points and soft points with uncertainty, (b) Segment-level control including trend and aggregated statistics (sum, average, etc.).

Methods for tackling subsets of the TSE challenge exist. For instance, control using provided trends in data can be achieved using models GANs (Yoon et al., 2019; Baasch et al., 2021), VAEs (Lee et al., 2023; Sommers et al., 2024), Diffusion Models (Ang et al., 2023; Tashiro et al., 2021; Yang et al., 2023; Cao et al., 2024; Tian et al., 2024; Ren et al., 2024; Adib et al., 2024) and editing skills in Table 1. Diffusion models have also been applied to achieving point-wise control (Coletta et al., 2023).

Table 1. Previous works for Time Series Editing. The RCGAN* and TimeGAN* adopt additional controls (Coletta et al., 2023)
.

Method	**Fixed Point**	**Soft Point**	**Trend**	**Statistics**	**Train with Condition**
GAN Models					
RCGAN* (Esteban et al., 2017)	✓	✗	✓	✓	✓
TimeGAN* (Yoon et al., 2019)	✓	✗	✓	✓	✓
WGAN-COP (Coletta et al., 2023)	✓	✗	✓	✓	✓
Diffusion Models					
DiffTime (Coletta et al., 2023)	✓	✗	✓	✓	✓
TimeWeaver (Narasimhan et al., 2024)	✗	✗	✓	✗	✓
TEdit (Jing et al., 2024)	✗	✗	✓	✗	✓
TimeBridge (Park et al., 2024)	✗	✗	✓	✗	✓
CocktailEdit (Our)	✓	✓	✓	✓	✗

However, none of these methods demonstrates satisfactory performance while being sufficiently fast and easy to use. They often incorporate prior knowledge by embedding provided signals into the model or training data, limiting flexibility for real-time human-centered modifications. Some methods choose to set a hard constraint on the learned distribution by embedding signals into the model architecture, e.g. time signals are injected into attention layers through additional embeddings, which limit the scope of this method and fail to consider possibilities of different kinds of human feedback/expected control signal (Yang et al., 2023; Cao et al., 2024; Tian et al., 2024; Ren et al., 2024; Zhang et al., 2024; Adib et al., 2024). In light of these considerations, we propose a novel method that overcomes these difficulties and can be used off the shelf with no additional training process. Our method utilizes diffusion models because they offer a mathematically rigorous framework that surpasses GANs in perceptual quality while avoiding adversarial training difficulties (Song et al., 2020b;a). This enables safe and verifiable injection of control signals - critical for achieving precise control in time series editing tasks.

Through theoretical analysis and extensive experiments, we demonstrate that our method achieves precise control while maintaining temporal coherence and distributional fidelity. By bridging the gap between pure generative modeling and practical time series editing needs, our work offers a flexible solution for human-in-the-loop applications like revenue forecasting with expert knowledge integration and scenario analysis. Our key contributions include:

- First unified framework for multi-grained TSE that enables point-wise and segment-wise manipulation of temporal patterns only on the inference stage
- Patching time series with the confidence-weighted target points simplifies human-in-loop modification with linear feedback under theoretical guarantees. Control temporal segments with aggregated statical properties.
- Our bottom-up methods can be extended and applied simultaneously to more points, and segments for longer time series in a conflict-free manner.

2. Preliminaries

2.1. Problem Formulation

The objective of TSE is to generate time series data that replicate the statistical properties of real-world sequences while adhering to specific user-defined controls. Given a set of time series $S = \{\mathbf{x}_i\}_{i=1}^N$, where each $\mathbf{x}_i \in \mathbb{R}^{L\times D}$ (L is the sequence length, D is the number of features), we aim to develop a model f_θ that learned from S and parameterized by θ such that: $\mathbf{x} = f_\theta(\mathbf{C})$, $\mathbf{C}$ represents the prior conditions. The model should be able to generate time series $\mathbf{x}$ that satisfies both the learned distribution and the provided constraints.

2.2. TSE Decomposition and Challenges

TSE is an umbrella term embodying difficulties from traditional time series tasks: prediction, imputation, and generation. However, while these classical tasks operate under specific, disjoint conditions – prediction uses historical data up to time t, imputation relies on partially observed segments, and unconditional generation requires no prior data – TSE must handle hybrid scenarios with multiple constraints.

Such complexity is divided into three dimensions: (1) temporal granularity (point-wise, segment-wise, and whole-series operations), (2) conditioning type (observed values, user-defined constraints, and learned patterns), and (3) transformation scope ($\mathcal{X}$ for temporal range and $\mathcal{Y}$ for value constraints). Decomposing TSE into these three orthogonal components allows us to systematically handle editing operations across scales while maintaining consistency between local modifications and global patterns.

Naturally, methods are also suggested to support extension from point-wise to segment-wise operations, and ultimately to whole-series transformations. Value constraints should incorporate both explicit user-defined targets and implicit constraints inferred from underlying models, providing flexibility while preserving time series characteristics.

2.3. Diffusion Models as Backbone

Diffusion models enable data generation through denoising, avoiding GANs' training instabilities and VAEs' reconstruction limitations (Ho et al., 2020; Pinheiro Cinelli et al., 2021; Goodfellow, 2016). The unique temporal dependencies and multi-scale patterns inherent in time series data make controlled generation a difficult task. Diffusion models, particularly DDPMs, present a solution as their iterative nature enables control at each denoising step. Moreover, classifier-free guidance and classifier-based modeling provide theoretical guarantees for this controlled generation. These properties allow us to achieve generation with distribution consistency and thus preserve important local and global time series properties inherent in the data. With the use of DDPMs, we developed a strategy to support editing constraints across temporal granularity, the basis of all the complex tasks that our work handles.

2.4. Diffusion Models: DDPM and Conditional

Denoising Diffusion Probabilistic Models (DDPM) Denoising Diffusion Probabilistic Models (DDPM) (Ho et al., 2020) approximate a data distribution $q(\mathbf{x})$ by gradually adding noise to data samples and then learning to reverse this noising process. The forward process is defined as a Markov chain:

$$q(\mathbf{x}_{1:K} \mid \mathbf{x}_0) = \prod_{k=1}^{K} q(\mathbf{x}_k \mid \mathbf{x}_{k-1}) \tag{1}$$

$$q(\mathbf{x}_k \mid \mathbf{x}_{k-1}) = \mathcal{N}\Big(\mathbf{x}_k; \sqrt{1-\beta_k}\, \mathbf{x}_{k-1}, \beta_k \mathbf{I}\Big), \tag{2}$$

where $\beta_k \in [0,1]$ controls the noise variance at each step. The reverse process is modeled by a parameterized Gaussian (Ho et al., 2020; Meijer & Chen, 2024):

$$p_\theta(\mathbf{x}_{k-1} \mid \mathbf{x}_k) = \mathcal{N}\Big(\mathbf{x}_{k-1}; \boldsymbol{\mu}_\theta(\mathbf{x}_k, k), \sigma_k^2 \mathbf{I}\Big). \tag{3}$$

To generate samples conditioned on extra inputs $\mathbf{C}$ (e.g., labels or prompts), Denoising Diffusion models augment the reverse process:

$$p_\theta(\mathbf{x} \mid \mathbf{C}) = \prod_{t=1}^{T} p_\theta(\mathbf{x}_{t-1} \mid \mathbf{x}_t, \mathbf{C}), \tag{4}$$

where

$$p_\theta(\mathbf{x}_{t-1} \mid \mathbf{x}_t, \mathbf{C}) = \mathcal{N}\big(\mathbf{x}_{t-1};\, \mu_\theta(\mathbf{x}_t, t, \mathbf{C}),\, \Sigma_\theta(\mathbf{x}_t, t)\big). \tag{5}$$

3. CocktailEdit

To tackle the multi-grained TSE task, we propose the CocktailEdit that integrates point-wise and segment-wise controls, which includes two control mechanisms: (1) a confidence-weighted point control (anchor control) for precise point specification, and (2) an enhanced classifier-based control for managing segment-level aggregated statistical properties. These mechanisms are implemented during the reverse diffusion process and can be used simultaneously, enforcing constraints across different granularities. A complete table of notations is included in Appendix A.1.

3.1. Point-Wise Control: Anchors with Confidence

Problem Setup Point-wise control can be formulated as a constrained imputation task. Given a time series $\mathbf{x}$ with both observed values $\mathbf{x}_{\text{ob}}$, called **anchors**, at known indices $\Omega(\mathbf{x})$ and target values $\mathbf{x}_{\text{ta}}$ which is the final target output, we aim to synthesize the target values using a diffusion model $p_\theta(\mathbf{x})$ trained on complete data while respecting the constraints. Formally, we define point-wise control constraints as: $\mathbf{C}_{\text{point}} = \{(\mathbf{t}_i, \mathbf{v}_i, \mathbf{c}_i, \mathbf{w}_i)\}_{i=1}^N$, where $\mathbf{t}_i \in \{1, \ldots, L\}$ specifies the time index, $\mathbf{v}_i \in \mathbb{R}$ defines the expected value, $\mathbf{c}_i \in \{1, \ldots, D\}$ indicates the feature index, and $\mathbf{w}_i \in \mathbb{R}$ represents the confidence level.

3.1.1. Float-Mask Imputation

Replace-Based Masking In Diffusion-TS and Diffwave (Yuan & Qiao, 2024; Kong et al., 2020), the infilling method for conditional sampling is based on replace-based imputation with a diffusion model. Thus, we adopt the replace-based imputation method as the initial point (Song et al., 2020b). For replace-based imputation, observed values are fixed at each step via the forward process, while missing values are iteratively refined with the diffusion model. By injecting exact samples of the known values into the latent sequence, the update steps for unknown dimensions gradually conform to the observed data distribution.

$$q\big(\mathbf{x}_{\text{ob}}^t \mid \mathbf{x}_{\text{ob}}^0\big) = \mathcal{N}\left(\mathbf{x}_{\text{ob}}^t; \sqrt{\overline{\alpha}_t}\,\mathbf{x}_{\text{ob}}^0, (1-\overline{\alpha}_t)\mathbf{I}\right), \tag{6}$$

$$\mathbf{x}_{\text{ta}}^t = \mathbf{x}_{\text{ta}}^{t+1} - \sqrt{\beta_t}\,\nabla_{\mathbf{x}_{\text{ta}}^{t+1}} \log p_\theta\big(\mathbf{x}_{\text{ta}}^{t+1} \mid \mathbf{x}_{\text{ta}}^{t+2}, \mathbf{x}_{\text{ob}}^t\big), \tag{7}$$

where $\overline{\alpha}_t = \prod_{i=1}^{t}(1-\beta_i)$.

Confidence-Based Masking How can we leverage the controllability of the aforementioned method but increase its flexibility to align users' requirements and expected output? We can treat injecting $\mathbf{x}_{\text{ob}}$ as adding a series of discrete masks $\mathbf{m} \in \{0, 1\}$ for $\mathbf{x}_{\text{ta}}$ and $\mathbf{x}_{\text{ob}}$ at each time step, i.e.

$$\mathbf{x}^t = \mathbf{m} \odot \mathbf{x}_{\text{ob}}^t + (1-\mathbf{m}) \odot \mathbf{x}_{\text{ta}}^t. \tag{8}$$

A natural extension is to consider continuous masks $\mathbf{m} \in [0,1]^{L\times D}$ for better generalization instead of $\mathbf{m} \in \{0,1\}^L$. The continuous mask allows for a smooth linear combination of observed data with model-generated updates, providing point-wise confidence weighting (anchor control). Then now the $\mathbf{C}_{\text{point}}$ can be reparameterzied as following: the $\mathbf{x}_i, \mathbf{y}_i, \mathbf{c}_i$ are grouped as the $\mathbf{x}_{\text{ob}}^0$ and the combined $\mathbf{w}_i$ is the float mask $\mathbf{m}$, which is restricted to $\mathbf{w}_i \in [0, 1]$ and $\mathbf{m} \in [0,1]^{L\times D}$. When $\mathbf{w}_i = 1$, the observed data is preserved, and when $\mathbf{w}_i = 0$, the model-generated data is retained.

Linear Controllability For output-oriented tasks, the relationship between user input and actual changes must be predictable and intuitive. Consider the iterative reverse process from time $\mathbf{x}^T$ down to $\mathbf{x}^0$ under a confidence mask $\mathbf{m} \in [0,1]^{L\times D}$. At each step $t \to t-1$, let $\mathbf{x}^t = \mathbf{m} \odot \mathbf{x}_{\text{ob}}^t + \big(1-\mathbf{m}\big) \odot \mathbf{x}_{\text{ta}}^t$. **Base case** ($t = T$): $\mathbf{x}^T$ is Gaussian noise by definition. **Inductive step**: Assume $\mathbf{x}^t$ is updatied for last timestep t; the reverse diffusion update refines $\mathbf{x}_{\text{ta}}^t$ via $\mathbf{x}_{\text{ta}}^{t-1} \leftarrow \mathbf{x}_{\text{ta}}^t - \sqrt{\beta_{t-1}}\,\nabla_{\mathbf{x}_{\text{ta}}^t} \log p_\theta(\ldots)$, while $\mathbf{x}_{\text{ob}}^{t-1}$ remains fixed (replace-based or float-masked). Hence $\mathbf{x}^{t-1} = \mathbf{m} \odot \mathbf{x}_{\text{ob}}^{t-1} + \big(1-\mathbf{m}\big) \odot \mathbf{x}_{\text{ta}}^{t-1}$, preserving the same linear form. Thus by induction, each reverse step remains a linear combination, and as $\mathbf{m} \to 1$ the final sample converges to the anchor $\mathbf{x}_{\text{ob}}$ under intensity described in $\mathbf{m}$.

With such provable linearity, the confidence mask aligns closely with human intuition regarding the expected linear behaviour of the change, ensuring better alignment of subsequent changes and accommodating user-defined constraints.

3.1.2. Advanced Float-Mask Control

While the proposed float-mask imputation provides a foundational mechanism for bridging the observed point to the final target data, more effective control mechanisms can be introduced to enhance the model's performance.

Time-Dependent Weighted Guidance To emphasize stronger control in later steps, we introduce the time-dependent weight:

$$\omega_t = \exp(-\gamma\,\frac{t}{\text{num\_timesteps}}), \tag{9}$$

which decays exponentially over time. This additional factor scales the mask value and gradient term during the inferencing stage, yielding stronger guidance at early timesteps and diminishing influence later in the denoising process.

Dynamic Error Adjustment on Float Mask Instead of a static mask, $\mathbf{m}$ can be dynamically adjusted during the reverse diffusion steps based on intermediate predictions or error metrics. This allows the model to adaptively allocate more attention to regions with higher uncertainty or discrepancy from desired constraints: $\mathbf{m}^{t-1} = \mathbf{m}^t + \Delta\mathbf{m}^t$, where $\Delta\mathbf{m}^t$ is a function of the current estimation error $\|\mathbf{x}_{\text{ta}}^t - \mathbf{x}_{\text{ta}}^{\text{target}}\|$ and with less inference steps.

3.2. Segment-Wise Control

3.2.1. Trend Control

From button to up, aggregated points can represent the trend of segments or even the whole time series. We observed that let $\mathbf{L}$ encode the relationship between time value and expected value in functions over this segment. If $\mathbf{L}$ is continuous, we can interpolate it to a discrete reference trend $\mathbf{l}_t \in \mathbb{R}$ for each time and corresponding values:

$$\mathbf{l}_t = \mathbf{L}_{t_s} + \frac{t-t_s}{t_e-t_s}(\mathbf{L}_{t_e} - \mathbf{L}_{t_s}), \quad t \in \{t_s, \ldots, t_e\}. \tag{10}$$

With simply extending groups of $(\mathbf{t}_i, \mathbf{v}_i, \mathbf{c}_{\text{trend}}, \mathbf{w}_i)$ for $\mathbf{C}_{\text{point}}$, which $\mathbf{t}_i \in \{t_s, \ldots, t_e\}$, $\mathbf{v}_i = \mathbf{l}_t$, we can consider multiple observed points as the trending control. The $\mathbf{m}_i$ can be adjusted according to the user's requirements.

Hierarchical Masking for Multi-Scale Control Continuing from trend control, to handle different temporal scale conflicts on $\mathbf{C}_{\text{point}}$, hierarchical masking can be employed. With multiple masks at varying granularities (e.g., local, segment, global), to control the diffusion process at different temporal resolutions. The combined mask $\mathbf{m}$ is obtained by merging masks from each hierarchy level:

$$\mathbf{m} = \lambda_1 \mathbf{m}_{\text{local}} + \lambda_2 \mathbf{m}_{\text{segment}} + \lambda_3 \mathbf{m}_{\text{global}}, \tag{11}$$

where λ_i are weighting coefficients ensuring that the combined mask maintains values within $[0, 1]$.

3.2.2. Statistics Control

For the statistics control, we can reformat the Segment-Wise Control: $\mathbf{C}_{\text{segment}} = \{(\mathbf{s}_j, \mathbf{e}_j, \mathbf{c}_j, \alpha_j, \mathbf{w}_j)\}_{j=1}^{M}$, where $\mathbf{s}_j, \mathbf{e}_j \in \{1, 2, \ldots, L\}$ are the start and end indices of the segment, and $\alpha_j \in \mathbb{R}$ is the parameters for aggregated functions, $\mathbf{w}_j$ are the weights of gradient intensity. **Score-Based DDPM for Controllable Generation** Guidance can further sampled toward desired attributes for Section 2.4:

$$\mathbf{x}_{t-1} = \mu_\theta(\mathbf{x}_t, t, \mathbf{C}) + \Sigma_\theta(\mathbf{x}_t, t)\, \nabla_{\mathbf{x}_t} \log p_\phi(\mathbf{C} \mid \mathbf{x}_t), \tag{12}$$

allowing controlled generation without retraining (Song et al., 2020b; Meijer & Chen, 2024). These works highlight how DDPMs, continuous-time Score-based SDE approaches, and conditional guidance strategies collectively enable powerful generative models that transform simple noise into complex data while remaining highly adaptable to additional constraints.

Additional Loss Term: Follow controllable diffusion models and (Coletta et al., 2023), we inject a penalty term $\mathcal{L}_{\text{pen}}(\mathbf{x}_t)$ enforcing aligning with the given condition $\mathbf{C}$:

$$\mathcal{L}_{\text{pen}} = -\beta \log p_\phi(\mathbf{y} \mid \mathbf{x}_t), \tag{13}$$

with a hyperparameter β. Then, minimizing $\mathcal{L}_{\text{pen}}$ effectively adds $-\beta\, \nabla_{\mathbf{x}_t} \log p_\phi(\mathbf{y} \mid \mathbf{x}_t)$ into the gradient flow. This mirrors the classifier-based guidance, bending the updated trajectory towards class $\mathbf{y}$ but without retraining θ. Hence, the final samples adhere to the classifier's preferences without additional model training. (Jing et al., 2024)

Example of aggregated function – Sum

$$\mathcal{L}_{\text{sum}[s_j:e_j]} = \left(\sum_{i=s_j}^{e_j} \mathbf{x}_{t,i} - S_{\text{target}[s_j:e_j]} \right)^2, \tag{14}$$

where s_j and e_j denote the start and end indices of the segment. The final loss term is:

$$\mathcal{L}_{\text{sum}} = \omega_t \sum \beta_{\text{sum}[s_j:e_j]} \mathcal{L}_{\text{sum}[s_j:e_j]}, \tag{15}$$

where $\beta_{\text{sum}[s_j:e_j]}$ is the weight for the sum control term, and ω_t is a timestep-dependent weight that yields stronger guidance in the later stages of the denoising process. For matching the $\mathbf{C}_{\text{segment}}$, the $\mathbf{C}_{\text{segment}}$ can be reparameterized as $\mathbf{C}_{\text{segment}} = \{(\mathbf{s}_j, \mathbf{e}_j, \mathbf{c}_j, \alpha_j, \mathbf{w}_j)\}_{j=1}^{M}$, where α_j is the expected aggregate statistic, and $\mathbf{w}_j$ is the weight for the segment-wise control term.

3.3. Multi-Grained Control

By integrating anchor and statistics controls on point- and segment-level, Algorithm 1 presents our unified denoising control framework for generalized DDPMs. Throughout the denoising process, we interleave point-wise floating mask control with segment-wise statistical control to gradually guide the denoising trajectory, requiring no model retraining or fine-tuning.

Algorithm 1 DDPM Denoising for Multi-Grained TSE

```
Require: Gradient scale $\eta$, trade-off coefficient $\gamma$, conditional data $\mathbf{x}_a$, time-dependent weight $\omega_t$
Initialize $\mathbf{x}_T \sim \mathcal{N}(\mathbf{0}, \mathbf{I})$
for $t = T$ to 1 do
    // Step 1: Predict and Refine Sample
    $[\hat{\mathbf{x}}_a, \hat{\mathbf{x}}_b] \leftarrow p_\theta(\mathbf{x}_t, t, \theta)$
    $\mathcal{L}_1 = \|\mathbf{x}_a - \hat{\mathbf{x}}_a\|_2^2$
    $\mathbf{x}_{t-1} \leftarrow \mathcal{N}\big(\mu(p_\theta(\mathbf{x}_t, t, \theta), \mathbf{x}_t), \Sigma\big)$
    $\mathcal{L}_2 = \|\mathbf{x}_{t-1} - \mu(p_\theta(\mathbf{x}_t, t, \theta), \mathbf{x}_t)\|_2^2 / \Sigma$
    // Step 2: Statistics Control
    $\mathcal{L}_{statistics} = \omega_t \sum \beta_{\text{sum}[s_j:e_j]} \mathcal{L}_{\text{sum}[s_j:e_j]}$
    $\tilde{\mathbf{x}}_0 = p_\theta(\mathbf{x}_t, t, \theta) + \eta \nabla_{\mathbf{x}_t}(\mathcal{L}_1 + \gamma \mathcal{L}_2 + \mathcal{L}_{statistics})$
    $\mathbf{x}_{t-1} \leftarrow \mathcal{N}\big(\mu(\tilde{\mathbf{x}}_0, \mathbf{x}_t), \Sigma\big)$
    // Step 3: Anchor Control
    $\mathbf{x}_{t-1} \leftarrow \omega_t \mathbf{m}^{\text{ob}} \odot \mathbf{x}_t^{\text{ob}} + (1 - \omega_t \mathbf{m}^{\text{ob}}) \odot \mathbf{x}_{t-1}$
end for
```

4. Experiments

4.1. Datasets

Our evaluation employs four diverse datasets across real-world and simulated scenarios. Table 2 summarizes the dataset specifications. The datasets include three real-world sources: ETTh [3] for electricity transformer measurements, fMRI [4] for blood-oxygen-level-dependent time series and Revenue dataset. The private Revenue dataset is sourced internally, containing revenue and other two features of hundreds of released video games. The simulated Sines dataset (Yoon et al., 2019) is generated with varying frequencies, amplitudes, and phases.

Table 2. Dataset specifications summarizing the data sources, sequence lengths, and dimensionality of four used datasets.

Dataset	Type	Source	Length	Features
ETTh	Real-world	Electricity transformer	24	28
fMRI	Real-world	BOLD time series	24	50
Revenue	Real-world	Game sales	365	3
Sines	Simulated	Synthetic waves	24	5

4.2. Experimental Setup

Following the infilling training setup of the Diffusion-TS framework (Yuan & Qiao, 2024), we adopt the CSDI (Tashiro et al., 2021) and Diffusion-TS (Yuan & Qiao, 2024) as fundamental models for our method.

[3] https://github.com/zhouhaoyi/ETDataset

[4] https://www.fmrib.ox.ac.uk/datasets/netsim

For inference, our method allows applying it separately to each channel, revealing channel dependencies. The training stage uses the entire dataset in a multivariate time series aligned with the community. For all experiments, control signals were applied exclusively to the first channel ($\mathbf{c} = 0$) to observe inter-channel influences while enabling multi-channel extensibility. All figures and results are based on the first channel unless stated otherwise. Training parameters and inference settings are expressed in Appendix B, such as choosing anchors and confidence scores.

4.3. Evaluation Metrics

We employ multiple metrics across two key aspects: control accuracy and distribution quality. For control accuracy, we measure: (i) **Mean Absolute Difference (MAD)** between generated and target values at anchor points, defined as $\text{MAD} = \frac{1}{N}\frac{1}{A}\sum_{i=1}^{N}\sum_{j=1}^{A}\left|x_{\text{cond gen}(i,j)} - x_{\text{target}(i,j)}\right|$; and (ii) **Statistic Control Result** to evaluate adherence to target statistic constraints. For example, the control target function is the sum of series, we directly observe the actual sum value change to validate the controllability. For distribution alignment check, followed by many works (Kong et al., 2020; Yuan & Qiao, 2024; Park et al., 2024; Ren et al., 2024), we utilize: (i) **Discriminative & Predictive scores** to assess how well-generated sequences replicate real data patterns, where discriminative score is $|$accuracy $- 0.5|$ and predictive score uses mean absolute error (MAE) between predictions and ground truth; (ii) **Context-FID score** which leverages a pre-trained TS2Vec model to measure distribution-level alignment, with lower scores indicating better similarity; and (iii) **Correlational score** that quantifies feature-level covariance preservation. We also complement these quantitative metrics with **Kernel Density Function** visualizations to provide qualitative insights into distribution alignment.

5. Results

5.1. Point-Wise Anchor Control

We conducted experiments to examine the relationship between anchor confidence values and prediction accuracy across different datasets. These experiments aim to validate our hypothesis that higher confidence values lead to more precise anchoring points and verify the behaviour at extreme confidence values (0.01 and 1.0).

Table 3 with the Diffusion-TS backbone demonstrates that increasing confidence values leads to a consistent MAD reduction across all datasets, ultimately converging to 0.0 at maximum confidence. This convergence at confidence = 1.0 validates our theoretical guarantee that maximum confidence forces the anchor point to be a fixed point. The monotonic and linear decrease of MAD with increasing confidence is visualized in Figure 2. The upper Figure 2 further confirm the theorem about linear controllability.

The second finding reveals that extreme target values (0.1 or 1.0) produce larger MAD values than moderate confidence levels (e.g., 0.5) across different datasets. For instance, on the fMRI Dataset, the MAD at $a_{target} = 0.1$ is 0.113, while at $a_{target} = 0.8$, it reduces to 0.052. This pattern, visible in Table 3, supports our hypothesis about the trade-off between very low and very high confidence values in anchor point selection. Comparing the MAD of the Original Dataset and Unconditional across the three target values, the anchor control approach demonstrates a smaller MAD even with a confidence score of 0.01. This indicates that anchor control helps generate time series data closer to the target value at a specified time. Furthermore, the pattern of largest and smallest MAD values aligns with those in the original and unconditional versions, suggesting that anchor control preserves the original distribution and MAD for each dataset while reducing its MAD magnitude.

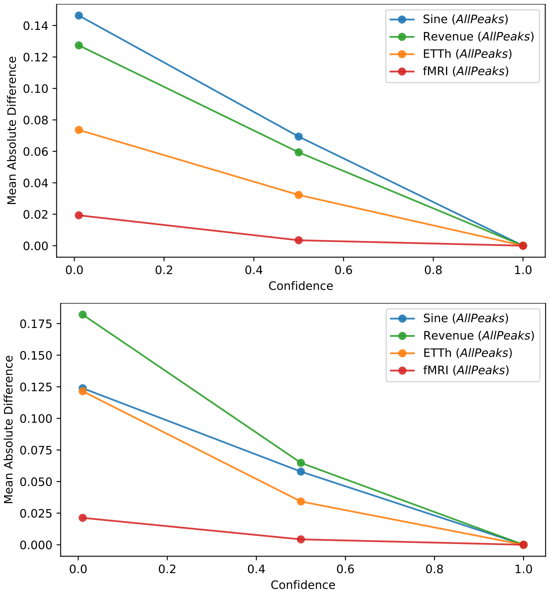

Figure 2. **Anchor Control** The influence of confidence across datasets. The lower figure is examined when enabling the dynamic error adjustment and time-depend weight, while the upper figure is not. "AllPeaks" means the averaged all experiments of anchor control. The model is Diffusion-TS, more in Appendix C.4

.

5.2. Segement-Wise Statistical Control

Our experiments investigate two key aspects of the aggregated statistic adjustment mechanism: (1) the effectiveness of different target values in steering the **segment sum** and **sequence sums**, and (2) the impact of **weight parameters** on control strength. These experiments aim to validate whether our method can reliably guide sequences toward desired sum targets while maintaining data fidelity.

Table 3. **Anchor Control** MAD of the given anchor indices in different setups of different confidence levels and target values.

Target Value \Confidence	Original	0.00 (Uncon)	0.01	0.50	1.00	Average
ETTh Dataset						
0.1	.0661	.0614	.0233	.0038	.0000	.0090
0.8	.7201	.7363	.0734	.0400	.0000	.0378
0.8	.5775	.6021	.1293	.0622	.0000	.0638
1.0	.7775	.8021	.2219	.1007	.0000	.1075
Average	.4988	.5102	.1274	.0594	.0000	
fMRI Dataset						
0.1	.4423	.4409	.0288	.0050	.0000	.0113
0.8	.2620	.2632	.0129	.0027	.0000	.0052
1.0	.4577	.4591	.0163	.0027	.0000	.0063
Average	.3873	.3877	.0193	.0035	.0000	
Sine Dataset						
0.1	.6530	.6617	.2511	.1116	.0000	.1209
0.8	.1466	.1455	.0700	.0377	.0000	.0359
1.0	.2470	.2383	.1179	.0588	.0000	.0589
Average	.3489	.3485	.1463	.0694	.0000	

Whole Sequence Sum As shown in Table 4, the controlled sequences consistently respond to different target values across all datasets. For the Revenue dataset, when targeting 150.0, the sequence sum increases significantly from 76.6 to 117.9, while targeting -100.0 reduces it to 52.7. Similar patterns are observed in other datasets - ETTh shows controlled variation from 1.5 to 11.1 (100) and 0.8 (-150), etc. Moreover, Revenue shows increasing steps: +2.705 from -100.0 to 20.0, +3.206 from 20.0 to 50.0, and +59.283 from 50.0 to 150.0. Both patterns demonstrate fine-grained control for smaller adjustments and the ability to make substantial changes when needed. Figures in Appendix D.1 visualize more controlled time series with different targets.

The weight parameter experiments reveal that varying weights from 1 to 100 produces only minor changes in the resulting sums. Target value rather than the control weight is the primary driver of loss-based control performance. Then, the weight parameters may be simplified in practical applications since they do not contribute substantially to control performance. The normalized trends in Figure 5.2 further support this observation.

Table 4. **Sum Control** Average summation value for various weights of sum control. "Original": the original training set; "Uncon": Unconditional generated samples. The **largest** and smallest MAD are labelled in each dataset.(Diffusion-TS)

.

Dataset	Original	Uncon	Target Value			
			-100.0	20.0	50.0	150.0
Sine	17.881	18.086	7.114	20.146	20.991	**21.031**
Revenue	80.194	76.619	52.675	55.380	58.585	**117.868**
ETTh	1.924	1.535	0.802	8.502	10.323	**11.102**
fMRI	12.990	12.980	4.675	17.192	19.811	**20.508**

Dataset	Original	Uncon	Weight Value			
			1	10	50	100
Sine	17.881	18.086	7.110	7.114	**7.117**	7.115
Revenue	80.194	76.619	**52.767**	52.675	52.741	52.725
ETTh	1.924	1.535	0.798	**0.802**	0.796	0.800
fMRI	12.990	12.980	4.678	4.675	4.677	**4.682**

Segment Sum To evaluate segment-wise control, we tested 3 segments: $(0.2L, 0.4L)$, $(0.4L, 0.6L)$, $(0.6L, 0.8L)$ with target value 150. Figure 4 shows that each controlled segment demonstrates increased sum adjustments. The effectiveness is particularly visible in the ETTh and Revenue datasets. The controlled segments exhibit clear increases in area under the curve when targeting higher sums with Diffusion-TS, while the effect of CSDI controlling is not obvious.

5.3. Distribution Alignment

Table E demonstrates that Diffusion-TS achieves better distribution matching than CSDI in unconditional generation across all datasets, with scores approaching 0, particularly for ETTh (0.034) and Sines (0.019). However, both Anchor and Statistics controls lead to increased divergence, suggesting a trade-off between control and distribution preservation. The comprehensive table can be found in Appendix C.3.

Table 5. Discriminative score for our method on CSDI and Diffusion-TS (DTS). The lower the score, the more similar the distribution of generated time series with original datasets.

Model	Control	ETTh	Revenue	fMRI	Sines
Our - CSDI	**Unconditional**	0.361±0.007	0.245±0.164	0.306±0.021	0.017±0.007
	Anchor	0.470±0.003	0.313±0.046	0.482±0.004	0.430±0.038
	Statistics	0.373±0.007	0.272±0.055	0.377±0.019	0.034±0.007
Our - DTS	**Unconditional**	0.034±0.026	0.209±0.185	0.089±0.033	0.019±0.008
	Anchor	0.437±0.004	0.393±0.030	0.495±0.001	0.460±0.011
	Statistics	0.477±0.003	0.426±0.032	0.498±0.001	0.451±0.029

5.4. Time Efficiency Analysis

Our time efficiency analysis from Table 6 reveals CSDI's computational advantage, processing samples 3-9x faster than Diffusion-TS across all datasets. The runtime scales primarily with sequence length, as evidenced by the Revenue dataset's higher processing times. Notably, both anchor and statistics-based controls add minimal computational overhead, maintaining consistent performance across control configurations. Feature dimensionality has a secondary but observable impact on processing time.

Table 6. Time efficiency analysis of our method compared on CSDI and Diffusion-TS (DTS). The results show the average time per sample for each dataset and control configuration. 500 examples per batch with an average of 5 batches.

Method	Dataset			Time Per Sample (ms)		
	Name	Seq	Features	Uncon	Anchor	Statistics
Our - CSDI	Energy	24	28	**0.064±0.000**	0.064±0.004	0.064±0.001
	fMRI	24	50	0.116±0.000	**0.115±0.001**	0.117±0.001
	Revenue	365	3	**1.000±0.001**	1.016±0.022	1.001±0.013
	Sines	24	5	0.018±0.000	0.017±0.001	0.018±0.001
Our - DTS	Energy	24	28	**0.278±0.017**	0.304±0.002	0.292±0.001
	fMRI	24	50	0.376±0.154	**0.232±0.883**	0.549±0.274
	Revenue	365	3	**9.163±0.411**	9.580±5.126	9.223±0.044
	Sines	24	5	**0.046±0.015**	0.059±0.020	0.048±0.001

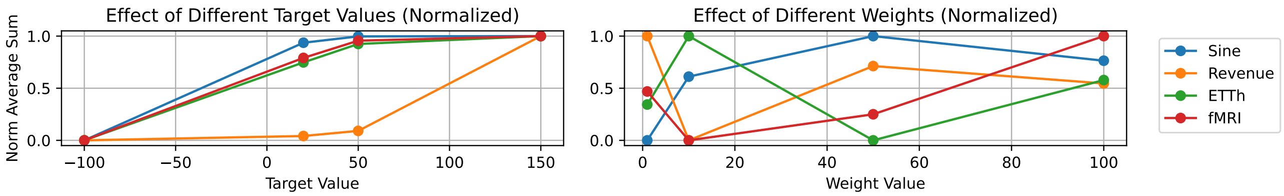

Figure 3. Normalized comparison of sum control effectiveness across datasets. Values are scaled relative to dataset-specific ranges to enable direct comparison between different domains. Lines show progressive convergence toward target sums. (Diffusion-TS)

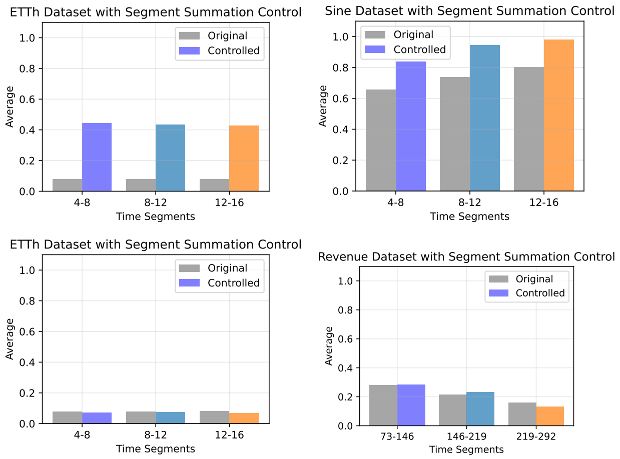

Figure 4. Segment-wise sum control results for different datasets. The shaded area represents the controlled segment, with the corresponding average sum value across different time segments. The datasets from left to right are: ETTh, Revenue, fMRI and Sine.

6. Related Work

Traditional generative tasks employed GANs (Wiese et al., 2020; Nguyen & Quanz, 2021; Yoon et al., 2019; Baasch et al., 2021), VAEs (Desai et al., 2021; Lee et al., 2023), Diffusion Models (Ang et al., 2023; Tashiro et al., 2021; Yang et al., 2023; Cao et al., 2024; Tian et al., 2024; Ren et al., 2024; Adib et al., 2024; Jing et al., 2024; Zhou et al., 2023), and Flow Matching (Hu et al., 2024), establishing foundational techniques for synthetic time series generation.

6.1. Time Series Generation Models

TimeGAN (Yoon et al., 2019) introduced temporal-aware adversarial training, while subsequent works like C-TimeGAN (Baasch et al., 2021) and CGAN-TS (Miao et al., 2021) incorporated conditional generation capabilities. Recent Transformer-based architectures (Sommers et al., 2024; Wen et al., 2023) have further enhanced representation capabilities for temporal patterns. Early control mechanisms focused on global attributes through models like TimeVAE (Desai et al., 2021), TimeGAN (Yoon et al., 2019), and C-TimeGAN (Baasch et al., 2021). Recent advances include hierarchical approaches (Torres et al., 2021) and attention-based mechanisms (Liu & Wang, 2024). Notably, CGAN-TS (Miao et al., 2021) and ControlTS (Wang et al., 2024) introduced attribute-based and temporal feature control.

6.2. Diffusion Models for Time Series

The adaptation of diffusion models to time series data has seen rapid advancement through several key developments. Early works like TimeGrad (Rasul et al., 2021) and CSDI (Tashiro et al., 2021) established the viability of diffusion models for temporal data, particularly in handling missing value imputation and uncertainty quantification. These foundations led to architectural innovations including TimeDiT (Cao et al., 2024), which introduced specialized temporal attention mechanisms, and Diff-MTS (Ren et al., 2024), which enhanced multivariate time series generation through improved cross-channel modeling.

Recent advances have focused on both architectural improvements and control mechanisms. The Latent Diffusion Transformer (Feng et al., 2024) demonstrated efficient generation through compressed latent spaces, while RATD (Liu et al., 2024) introduced robust attention mechanisms for handling temporal dependencies. Score-CDM (Zhang et al., 2024) and DiffusionBridge (Park et al., 2024) advanced controlled generation through score-based approaches and bridge construction methods respectively. These developments have enabled successful applications across diverse domains, from healthcare monitoring (Adib et al., 2024) and industrial systems (Tian et al., 2024) to financial forecasting (Yang et al., 2023; Hamdouche et al., 2023).

While existing methods show promise, they primarily focus on global trend control and distribution matching, lacking, fine-grained control at the individual timestamp level except DiffTime and Guided-DiffTime (Coletta et al., 2023), working on the point-wise constrained time series generation. However, their points control needs additional training.

7. Conclusion

We present the CocktailEdit for generalized Time Series Editing that enables fine-grained control and global statistical manipulation without model retraining. It is achieved via float masking and score-based guidance for statistical properties. The interleaving nature of the two mechanisms allows them to be seamlessly combined, enabling sophisticated editing operations that respect both fine-grained constraints and coarse-grained properties. This makes our framework particularly suitable for real-world applications where domain experts need to incorporate specific knowledge while maintaining overall statistical validity. Figure G demonstrates the practical interactive editing interface to enable the intuitive manipulation of temporal data like Photoshop. The control mechanism is not perfect and the obvious distribution drift still exists. Our method can be further improved by incorporating more advanced control mechanisms and carefully considering the trade-off between control precision and distribution preservation.

Impact Statement

Our work introduces controlled generation techniques for time series data that could significantly impact both research and practical applications. This framework enables precise manipulation of temporal data through anchor points and statistical controls, potentially transforming how we approach scenario analysis, forecasting, and anomaly detection in fields like financial modeling, healthcare monitoring, and energy systems.

However, we acknowledge important limitations and risks. The trade-off between control precision and distribution preservation requires careful consideration in practical applications. Additionally, while our method shows promise on most datasets, its consistent failure on revenue data highlights the need for further research into domain-specific adaptations.

Looking forward, this work opens new directions for investigating the controlled generation of temporal data, with potential applications in simulation, testing, and data augmentation. We hope our framework will serve as a foundation for developing more sophisticated and reliable methods for time series manipulation while emphasizing the importance of responsible development and application of such technologies.

References

Adib, E., Fernandez, A. S., Afghah, F., and Prevost, J. J. Synthetic ecg signal generation using probabilistic diffusion models. *IEEE Access*, 11:75818–75828, 2024. doi: 10.1109/ACCESS.2023.3296542.

Alcaraz, J. M. L. and Strodthoff, N. Diffusion-based time series imputation and forecasting with structured state space models. *Version published by Transactions on Machine Learning Research in 2022 (TMLR ISSN 2835-8856) https://openreview.net/forum?id=hHiIbk7ApW*, August 2022. doi: 10.48550/ARXIV.2208.09399.

Ang, Y., Huang, Q., Bao, Y., Tung, A. K. H., and Huang, Z. Tsgbench: Time series generation benchmark. September 2023. doi: 10.48550/ARXIV.2309.03755.

Baasch, G., Rousseau, G., and Evins, R. A conditional generative adversarial network for energy use in multiple buildings using scarce data. *Energy and AI*, 5:100087, 2021. ISSN 2666-5468. doi: https://doi.org/10.1016/j.egyai.2021.100087. URL https://www.sciencedirect.com/science/article/pii/S2666546821000410.

Bao, Y., Ang, Y., Huang, Q., Tung, A. K. H., and Huang, Z. Towards controllable time series generation. March 2024. doi: 10.48550/ARXIV.2403.03698.

Cao, D., Ye, W., Zhang, Y., and Liu, Y. Timedit: General-purpose diffusion transformers for time series foundation model. September 2024. doi: 10.48550/ARXIV.2409.02322.

Coletta, A., Gopalakrishnan, S., Borrajo, D., and Vyetrenko, S. On the constrained time-series generation problem. In Oh, A., Naumann, T., Globerson, A., Saenko, K., Hardt, M., and Levine, S. (eds.), *Advances in Neural Information Processing Systems*, volume 36, pp. 61048–61059. Curran Associates, Inc., 2023.

Desai, A., Freeman, C., Wang, Z., and Beaver, I. Timevae: A variational auto-encoder for multivariate time series generation. November 2021. doi: 10.48550/ARXIV.2111.08095.

Esteban, C., Hyland, S. L., and Rätsch, G. Real-valued (medical) time series generation with recurrent conditional gans. June 2017. doi: 10.48550/ARXIV.1706.02633.

Feng, S., Miao, C., Zhang, Z., and Zhao, P. Latent diffusion transformer for probabilistic time series forecasting. *Proceedings of the AAAI Conference on Artificial Intelligence*, 38(11):11979–11987, Mar. 2024. doi: 10.1609/aaai.v38i11.29085. URL https://ojs.aaai.org/index.php/AAAI/article/view/29085.

Goodfellow, I. Nips 2016 tutorial: Generative adversarial networks. *arXiv preprint arXiv:1701.00160*, 2016.

Hamdouche, M., Henry-Labordere, P., and Pham, H. Generative modeling for time series via schrödinger bridge. April 2023. doi: 10.48550/ARXIV.2304.05093.

Ho, J., Jain, A., and Abbeel, P. Denoising diffusion probabilistic models. June 2020. doi: 10.48550/ARXIV.2006.11239.

Hu, Y., Wang, X., Wu, L., Zhang, H., Li, S. Z., Wang, S., and Chen, T. Fm-ts: Flow matching for time series generation. November 2024. doi: 10.48550/ARXIV.2411.07506.

Jing, B., Gu, S., Chen, T., Yang, Z., Li, D., He, J., and Ren, K. Towards editing time series. In *The Thirty-eighth Annual Conference on Neural Information Processing*

Systems, 2024. URL https://openreview.net/forum?id=qu5NTwZtxA.

Kong, Z., Ping, W., Huang, J., Zhao, K., and Catanzaro, B. Diffwave: A versatile diffusion model for audio synthesis. *arXiv preprint arXiv:2009.09761*, 2020.

Lee, D., Malacarne, S., and Aune, E. Vector quantized time series generation with a bidirectional prior model. March 2023. doi: 10.48550/ARXIV.2303.04743.

Li, Y., Lu, X., Wang, Y., and Dou, D. Generative time series forecasting with diffusion, denoise, and disentanglement. In Koyejo, S., Mohamed, S., Agarwal, A., Belgrave, D., Cho, K., and Oh, A. (eds.), *Advances in Neural Information Processing Systems*, volume 35, pp. 23009–23022. Curran Associates, Inc., 2022.

Liu, J., Yang, L., Li, H., and Hong, S. Retrieval-augmented diffusion models for time series forecasting. October 2024. doi: 10.48550/ARXIV.2410.18712.

Liu, X. and Wang, W. Deep time series forecasting models: A comprehensive survey. *Mathematics*, 12(10), 2024. ISSN 2227-7390. doi: 10.3390/math12101504. URL https://www.mdpi.com/2227-7390/12/10/1504.

Meijer, C. and Chen, L. Y. The rise of diffusion models in time-series forecasting. January 2024. doi: 10.48550/ARXIV.2401.03006.

Miao, X., Wu, Y., Wang, J., Gao, Y., Mao, X., and Yin, J. Generative semi-supervised learning for multivariate time series imputation. In *Proceedings of the AAAI conference on artificial intelligence*, volume 35, pp. 8983–8991, 2021.

Narasimhan, S. S., Agarwal, S., Akcin, O., Sanghavi, S., and Chinchali, S. Time weaver: A conditional time series generation model. March 2024. doi: 10.48550/ARXIV.2403.02682.

Nguyen, N. and Quanz, B. Temporal latent auto-encoder: A method for probabilistic multivariate time series forecasting. In *Proceedings of the AAAI conference on artificial intelligence*, volume 35, pp. 9117–9125, 2021.

Park, J., Lee, S., Jeong, W., Choi, Y., and Lee, J. Leveraging priors via diffusion bridge for time series generation. August 2024. doi: 10.48550/ARXIV.2408.06672.

Pinheiro Cinelli, L., Araújo Marins, M., Barros da Silva, E. A., and Lima Netto, S. Variational autoencoder. In *Variational Methods for Machine Learning with Applications to Deep Networks*, pp. 111–149. Springer, 2021.

Rasul, K., Seward, C., Schuster, I., and Vollgraf, R. Autoregressive denoising diffusion models for multivariate probabilistic time series forecasting. In Meila, M. and Zhang, T. (eds.), *Proceedings of the 38th International Conference on Machine Learning*, volume 139 of *Proceedings of Machine Learning Research*, pp. 8857–8868. PMLR, 18–24 Jul 2021. URL https://proceedings.mlr.press/v139/rasul21a.html.

Ren, L., Wang, H., and Laili, Y. Diff-mts: Temporal-augmented conditional diffusion-based aigc for industrial time series toward the large model era. *IEEE Transactions on Cybernetics*, 54(12):7187–7197, 2024. doi: 10.1109/TCYB.2024.3462500.

Sommers, A., Cummins, L., Mittal, S., Rahimi, S., Seale, M., Jaboure, J., and Arnold, T. A survey of transformer enabled time series synthesis. June 2024. doi: 10.48550/ARXIV.2406.02322.

Song, J., Meng, C., and Ermon, S. Denoising diffusion implicit models. October 2020a. doi: 10.48550/ARXIV.2010.02502.

Song, Y., Sohl-Dickstein, J., Kingma, D. P., Kumar, A., Ermon, S., and Poole, B. Score-based generative modeling through stochastic differential equations. November 2020b. doi: 10.48550/ARXIV.2011.13456.

Tashiro, Y., Song, J., Song, Y., and Ermon, S. Csdi: Conditional score-based diffusion models for probabilistic time series imputation. In Ranzato, M., Beygelzimer, A., Dauphin, Y., Liang, P., and Vaughan, J. W. (eds.), *Advances in Neural Information Processing Systems*, volume 34, pp. 24804–24816. Curran Associates, Inc., 2021. URL https://proceedings.neurips.cc/paper_files/paper/2021/file/cfe8504bda37b575c70ee1a8276f3486-Paper.pdf.

Tian, M., Chen, B., Guo, A., Jiang, S., and Zhang, A. R. Reliable generation of privacy-preserving synthetic electronic health record time series via diffusion models. *Journal of the American Medical Informatics Association*, 31(11):2529–2539, 09 2024. ISSN 1527-974X. doi: 10.1093/jamia/ocae229. URL https://doi.org/10.1093/jamia/ocae229.

Torres, J. F., Hadjout, D., Sebaa, A., Martínez-Álvarez, F., and Troncoso, A. Deep learning for time series forecasting: A survey. *Big Data*, 9(1):3–21, February 2021. ISSN 2167-647X. doi: 10.1089/big.2020.0159.

Wang, Y., Wu, H., Dong, J., Liu, Y., Long, M., and Wang, J. Deep time series models: A comprehensive survey and benchmark. July 2024. doi: 10.48550/ARXIV.2407.13278.

Wen, H., Lin, Y., Xia, Y., Wan, H., Wen, Q., Zimmermann, R., and Liang, Y. Diffstg: Probabilistic spatio-temporal graph forecasting with denoising diffusion models. In *Proceedings of the 31st ACM International Conference on Advances in Geographic Information Systems*, pp. 1–12, 2023.

Wiese, M., Knobloch, R., Korn, R., and Kretschmer, P. Quant gans: deep generation of financial time series. *Quantitative Finance*, 20(9):1419–1440, 2020.

Yang, F., Yin, W., Wang, L., Li, T., Zhao, P., Liu, B., Wang, P., Qiao, B., Liu, Y., Björkman, M., Rajmohan, S., Lin, Q., and Zhang, D. Diffusion-based time series data imputation for cloud failure prediction at microsoft 365. In *Proceedings of the 31st ACM Joint European Software Engineering Conference and Symposium on the Foundations of Software Engineering*, ESEC/FSE '23, pp. 2050–2055. ACM, November 2023. doi: 10.1145/3611643.3613866.

Yoon, J., Jarrett, D., and van der Schaar, M. Time-series generative adversarial networks. In Wallach, H., Larochelle, H., Beygelzimer, A., d'Alché-Buc, F., Fox, E., and Garnett, R. (eds.), *Advances in Neural Information Processing Systems*, volume 32. Curran Associates, Inc., 2019. URL https://proceedings.neurips.cc/paper_files/paper/2019/file/c9efe5f26cd17ba6216bbe2a7d26d490-Paper.pdf.

Yuan, X. and Qiao, Y. Diffusion-ts: Interpretable diffusion for general time series generation. March 2024. doi: 10.48550/ARXIV.2403.01742.

Zhang, S., Wang, S., Miao, H., Chen, H., Fan, C., and Zhang, J. Score-cdm: Score-weighted convolutional diffusion model for multivariate time series imputation. May 2024. doi: 10.48550/ARXIV.2405.13075.

Zhou, L., Lou, A., Khanna, S., and Ermon, S. Denoising diffusion bridge models. September 2023. doi: 10.48550/ARXIV.2309.16948.

A. Methodology Additional Details

A.1. Summary of Variants

Table 7. Summary of variables and their Meanings

Symbol	Meaning
N	Number of time series
$\mathbf{x}_i \in \mathbb{R}^{L\times D}$	i-th time series, length L, dimension D
$S = \{\mathbf{x}_i\}_{i=1}^{N}$	Training dataset of time series
θ	Model parameters of f_θ
$\mathbf{C}$	Prior/conditioning input
T	Total forward/backward diffusion steps
K	Set of number of gradient steps per diffusion step
$\beta_k \in [0, 1]$	Noise variance schedule
$\mathbf{x}_t$	Noisy sample at diffusion step t
$\mathbf{t}_i$	Time index in the sample $\mathbf{x}$
$\mathbf{v}_i$	Corresponding $\mathbf{y}$ value of the time index in sample $\mathbf{x}$
μ_θ, σ_k^2	Mean and variance in reverse diffusion
$\Omega(\mathbf{x}), \overline{\Omega}(\mathbf{x})$	Observed and missing indices
$\mathbf{x}_{\text{ob}}, \mathbf{x}_{\text{ta}}$	Observed and target parts of a time series
$\mathbf{m} \in [0, 1]^{L\times D}$	Confidence/float mask
ω_t	Time-dependent weight in reverse steps
$\mathbf{C}_{\text{point}}$	Point-wise control with confidence
$\mathbf{C}_{\text{segment}}$	Segment-wise control constraints
$\mathcal{L}_{\text{sum}}, \mathcal{L}_{\text{pen}}, \mathcal{L}_{\text{statistics}}$	Loss terms enforcing constraints
$\gamma, \eta, \beta_{\text{sum}[s_j:e_j]}$	Additional scale factors for guidance

A.2. DDPM and Conditional Generation

Denoising Diffusion Probabilistic Models (DDPM) (Ho et al., 2020) approximate a data distribution $q(\mathbf{x})$ by gradually adding noise to data samples and then learning to reverse this noising process. The forward process is defined as a Markov chain:

$$q(\mathbf{x}_{1:K} \mid \mathbf{x}_0) = \prod_{k=1}^{K} q(\mathbf{x}_k \mid \mathbf{x}_{k-1}), \tag{16}$$

$$q(\mathbf{x}_k \mid \mathbf{x}_{k-1}) = \mathcal{N}\Big(\mathbf{x}_k; \sqrt{1-\beta_k}\,\mathbf{x}_{k-1}, \beta_k \mathbf{I}\Big), \tag{17}$$

where $\beta_k \in [0, 1]$ controls the noise variance at each step. In closed form, one may sample the noisy state $\mathbf{x}_k$ from

$$q(\mathbf{x}_k \mid \mathbf{x}_0) = \mathcal{N}\Big(\mathbf{x}_k; \sqrt{\alpha_k}\,\mathbf{x}_0, (1-\alpha_k)\mathbf{I}\Big), \tag{18}$$

with $\alpha_k = \prod_{i=1}^{k}(1-\beta_i)$. The reverse process is modeled by a parameterized Gaussian:

$$p_\theta(\mathbf{x}_{k-1} \mid \mathbf{x}_k) = \mathcal{N}\Big(\mathbf{x}_{k-1}; \boldsymbol{\mu}_\theta(\mathbf{x}_k, k), \sigma_k^2 \mathbf{I}\Big). \tag{19}$$

The loss can be simplified by predicting either the noiseless data or the added noise. In practice, predicting noise often improves performance, leading to

$$\boldsymbol{\mu}_\epsilon(\mathbf{x}_k, k) = \frac{1}{\sqrt{1-\beta_k}}\Big(\mathbf{x}_k - \frac{\beta_k}{\sqrt{1-\alpha_k}}\,\epsilon_\theta(\mathbf{x}_k, k)\Big), \tag{20}$$

$$L = \mathbb{E}\big[\|\epsilon - \epsilon_\theta(\mathbf{x}_k, k)\|^2\big], \tag{21}$$

where $\epsilon \sim \mathcal{N}(\mathbf{0}, \mathbf{I})$. (Ho et al., 2020; Meijer & Chen, 2024)

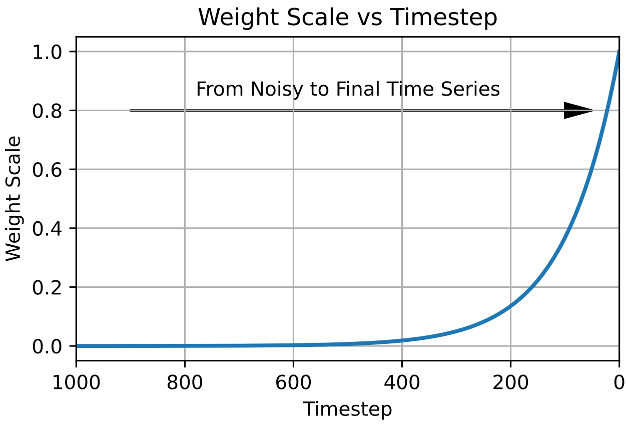

Figure 5. Time-dependent weight schedule during denoising process. The exponential decay ($\gamma = 5.0$) provides stronger control signals in later timesteps while allowing smoother adjustments near completion.

A.3. Time-Dependent Weight

A.4. Formal Proof of Float Mask Replacing

Proof. Let $p(x)$ be the jointly trained diffusion model over both observed and missing dimensions, and let $p(x_{ta} \mid x_{ob})$ be the target conditional distribution. Denote $p_t(x_{ob}^t, x_{ta}^t)$ as the distribution of (x_{ob}^t, x_{ta}^t) at iteration t. We show that as $t \to 0$, $p_t(x_{ta}^t \mid x_{ob}^t)$ converges to $p(x_{ta} \mid x_{ob})$.

I. Forward-Process Marginals. By construction, x_{ob}^t at each step is drawn from the forward process $q(x_{ob}^t \mid x_{ob}^0)$, which is a Gaussian transition that preserves the exact marginal of the known dimensions x_{ob}. Formally, for each t,

$$x_{ob}^t \sim \mathcal{N}\big(\sqrt{\bar{\alpha}_t}\, x_{ob}^0,\, (1 - \bar{\alpha}_t)\mathbf{I}\big).$$

Hence, $p_t(x_{ob}^t)$ remains consistent with the correct marginal distribution $\prod_{\Omega(x)} p(x_{ob})$.

II. Denoising of Missing Entries. The reverse step for missing entries x_{ta}^t is governed by

$$x_{ta}^t \leftarrow x_{ta}^{t+1} - \sqrt{\beta_t}\, \nabla_{x_{ta}^{t+1}} \log p_\theta(x_{ta}^{t+1} \mid x_{ta}^{t+2}, x_{ob}^t).$$

As shown in (Song et al., 2020b), iteratively applying the reverse diffusion steps in this score-based framework converges to sampling from $p(x_{ta} \mid x_{ob}^t)$.

III. Replace and Float-Mask Consistency. Whether we *replace* x_{ob}^t completely or *blend* it with a float mask $\mathbf{m}$:

$$x^t \;=\; \mathbf{m} \odot x_{ob}^t + (1 - \mathbf{m}) \odot x_{ta}^t,$$

the observed indices remain consistent with their forward-sampled values. This ensures that at every iteration, the joint distribution respects the known-data constraints. The 0.0 value in masks means no restriction on this point, and 1.0 means the fixed anchor point.

IV. Convergence to the Conditional. Consider $p_t(x_{ta}^t \mid x_{ob}^t)$. By the score-based argument (the forward-reverse chain forming a time-indexed Markov process), the mixture of denoising steps and partial resets of observed entries yields

$$\lim_{t \to 0} p_t(x_{ta}^t \mid x_{ob}^t) \;=\; p(x_{ta} \mid x_{ob}),$$

where the convergence follows from the fact that each reverse diffusion step corrects the noise injected in the forward pass, conditioned on the known x_{ob}^t.

Thus, replace-based or float-mask imputation each preserves x_{ob}'s marginals and iteratively refine x_{ta} until the distribution of the missing entries matches $p(x_{ta} \mid x_{ob})$. □

Implementation Details The float mask $\mathbf{m}$ can be adjusted to control the influence of observed data on the imputed sequence. By iterative sampling from the diffusion model and applying the floating mask, we can generate time series data that respects observed values while conforming to the correct conditional distribution.

1. **Initialize** x^T from Gaussian noise.
2. **For** $t = T$ down to 1:
   - *Forward-process sampling (for x^t_{ob}):* $x^t_{ob} \sim q\big(x^t_{ob} \mid x^0_{ob}\big)$.
   - *Denoise missing parts (for x^t_{ta}):* perform gradient step using $\log p_\theta$.
   - *Apply float mask (optional):* fuse observed and imputed regions via $\mathbf{m}$.

A.5. Improved Sampling

(Jing et al., 2024) mentioned the sampling algorithm follows reconstruction-guided conditional diffusion with adaptive gradient steps based on timestep t. Early timesteps receive more control updates to guide generation, while later stages use fewer updates to optimize efficiency. For balances quality with speed by focusing gradient corrections where they have the most impact - during the initial creative stages rather than final smoothing. The following is the used sampling Algorithm 2.

Algorithm 2 Improved DDPM Denoising for Multi-Grained TSE

```
Require: Gradient scale $\eta$, trade-off coefficient $\gamma$, conditional data $\mathbf{x}_a$, time-dependent weight $\omega_t$, times set $K$
Initialize $\mathbf{x}_T \sim \mathcal{N}(\mathbf{0}, \mathbf{I})$
for $t = T$ to 1 do
    for $k = 1$ to $K[t]$ do
        $[\hat{\mathbf{x}}_a, \hat{\mathbf{x}}_b] \leftarrow p_\theta(\mathbf{x}_t, t, \theta)$
        $\mathcal{L}_1 = \|\mathbf{x}_a - \hat{\mathbf{x}}_a\|_2^2$
        $\mathbf{x}_{t-1} \leftarrow \mathcal{N}\big(\mu(p_\theta(\mathbf{x}_t, t, \theta), \mathbf{x}_t), \Sigma\big)$
        $\mathcal{L}_2 = \|\mathbf{x}_{t-1} - \mu(p_\theta(\mathbf{x}_t, t, \theta), \mathbf{x}_t)\|_2^2 / \Sigma$
        $\mathcal{L}_{statistics} = \omega_t \sum \beta_{\mathrm{sum}[s_j:e_j]} \mathcal{L}_{\mathrm{sum}[s_j:e_j]}$
        $\tilde{\mathbf{x}}_0 = p_\theta(\mathbf{x}_t, t, \theta) + \eta \nabla_{\mathbf{x}_t}(\mathcal{L}_1 + \gamma \mathcal{L}_2 + \mathcal{L}_{statistics})$
    end for
    $\mathbf{x}_{t-1} \leftarrow \mathcal{N}\big(\mu(\tilde{\mathbf{x}}_0, \mathbf{x}_t), \Sigma\big)$
    $\mathbf{x}_{t-1} \leftarrow \omega_t \mathbf{m}^{\mathrm{ob}} \odot \mathbf{x}_t^{\mathrm{ob}} + (1 - \omega_t \mathbf{m}^{\mathrm{ob}}) \odot \mathbf{x}_{t-1}$
end for
```

B. Experiment Additional Details

Table 8. Training hyperparameters and settings for each dataset.

Method	Dataset			Training			Inference
	Name	Seq Length	Features	LR	Train Steps	Batch Szie	DDPM Timesteps
Our - CSDI	Energy	24	28	1.00E-03	25000	64	200
	fMRI	24	50	1.00E-03	15000	64	200
	Revenue	365	3	2.00E-03	2230	64	200
	Sines	24	5	1.00E-03	12000	128	50
Our - Diffusion-TS	Energy	24	28	1.00E-05	25000	64	1000
	fMRI	24	50	1.00E-05	15000	64	1000
	Revenue	365	3	2.00E-05	2230	64	500
	Sines	24	5	1.00E-05	12000	128	500

We run all training and inferencing of all experiments with NVIDIA L40S GPUs. All experiments are fixed on the random seed with 2024. Table 8 summarizes the training hyperparameters for each dataset and method. We use the Adam optimizer with a learning rate of 1.00×10^{-3} for CSDI and 1.00×10^{-5} for Diffusion-TS. The training steps are set to 25,000 for CSDI and 15,000 for Diffusion-TS. The batch size is 64 for CSDI and 128 for Diffusion-TS. The number of diffusion steps is set according to the different datasets.

For anchor point control, we placed anchor targets at normalized values $\mathbf{v}_{anchor} \in \{0.1, 0.8, 1.0\}$ at relative temporal positions $\mathbf{t}_{anchor} \in \{0.1L, 0.3L, 0.5L, 0.7L, 0.9L\}$. The confidence levels are set to $\mathbf{c}_{anchor} = \{0.01, 0.50, 1.0\}$ at the corresponding anchor indices, and the other positions were set to 0.0 during mask converting.

For the segment-wise control, we test on segments $\{(s, e)\}$ =$\{(0.2L, 0.4L), (0.4L, 0.6L), (0.6L, 0.8L),$ $(0, L)\}$, $(0, L)$ represents the whole sequence. We choose "sum" as the aggregated function, then $\alpha_{sum} \in \{-100, 20, 50, 100\}$ as the targeted aggregated statistics, weight $\beta_{sum} \in \{1, 10, 50, 100\}$. We note that baseline sums vary significantly between datasets due to sequence length and data scaling, we will include the various sequence length results, such $L \in \{96, 192, 384\}$ in the camera-ready version.

C. Anchor Control

C.1. Demonstrates

The following figures demonstrate the effectiveness of anchor control across different datasets varying this confidence and target value with Diffusion-TS and CSDI. We can see as the confidence increases, the model respects the anchor points more strictly.

C.1.1. Pure Float Mask Control (Diffusion-TS)

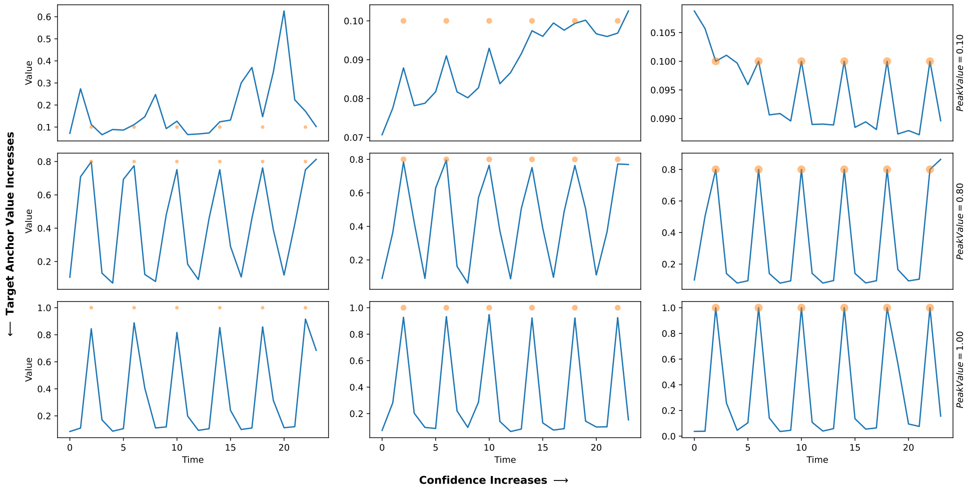

Figure 6. Demonstration of Anchor Control in ETTh datasets with multiple anchor points and confidences

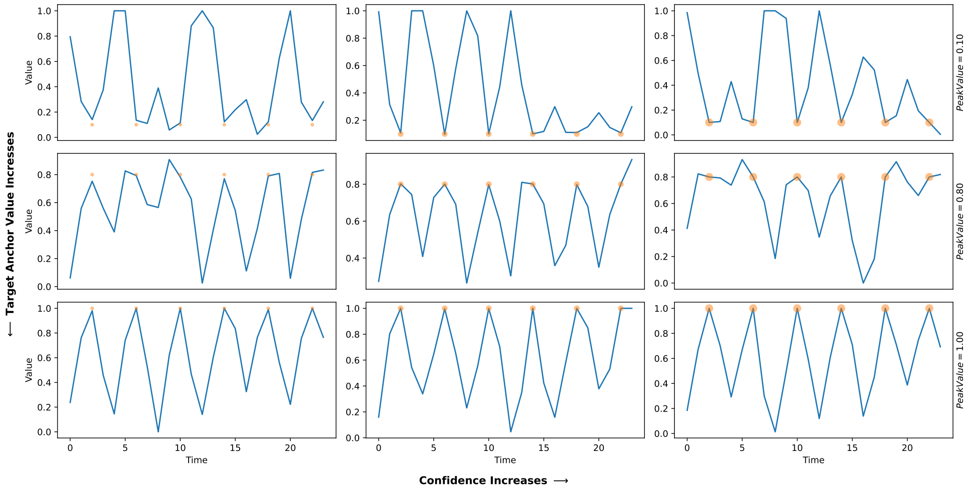

Figure 7. Demonstration of Anchor Control in fMRI datasets with multiple anchor points and confidences.

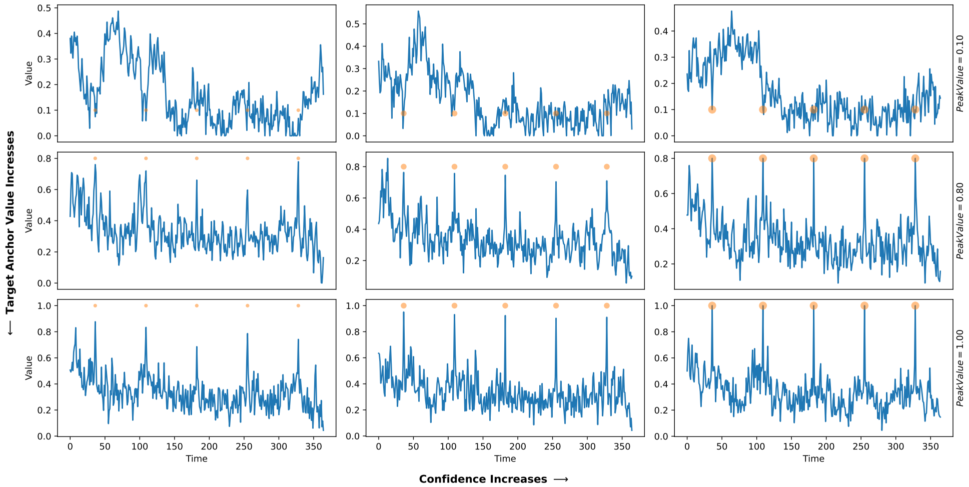

Figure 8. Demonstration of Anchor Control in Revenue datasets with multiple anchor points and confidences

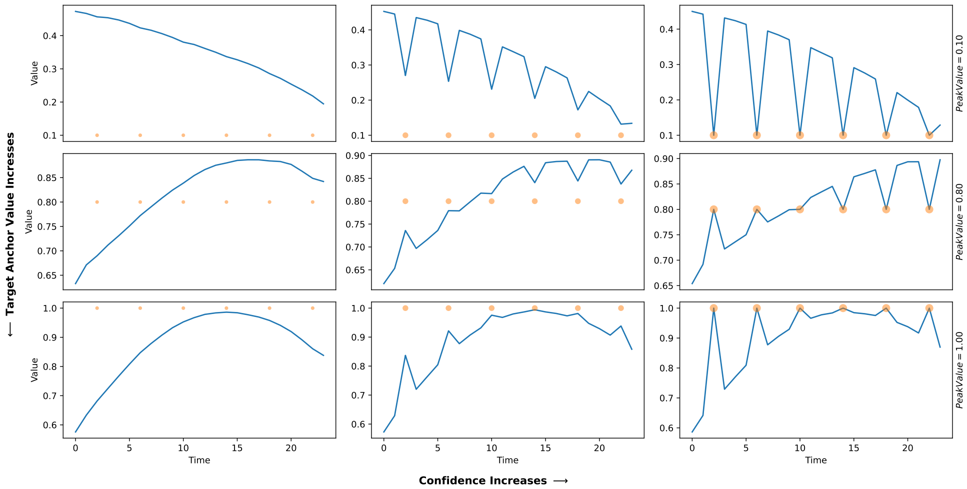

Figure 9. Demonstration of Anchor Control in Synthetic sine wave datasets with multiple anchor points and confidences

C.1.2. Float Mask Control with Extensions (Diffusion-TS)

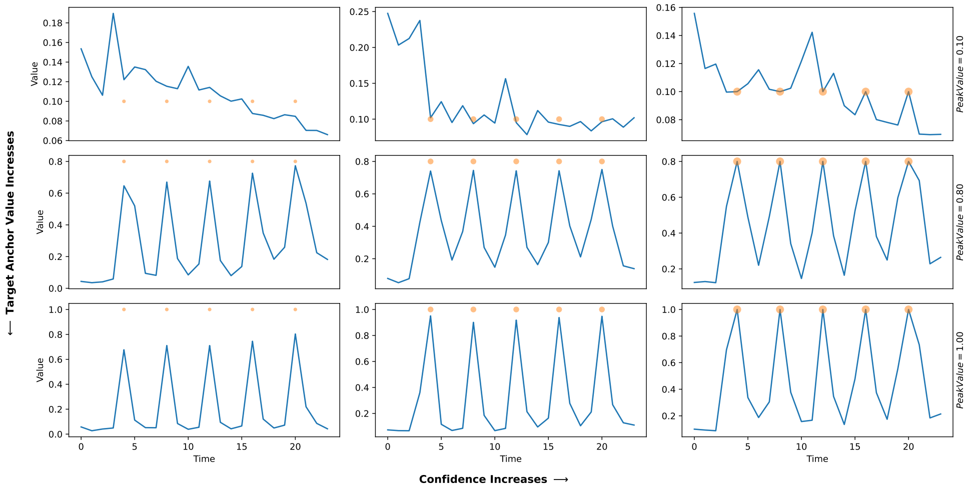

Figure 10. Demonstration of Anchor Control in ETTh datasets with multiple anchor points and confidences

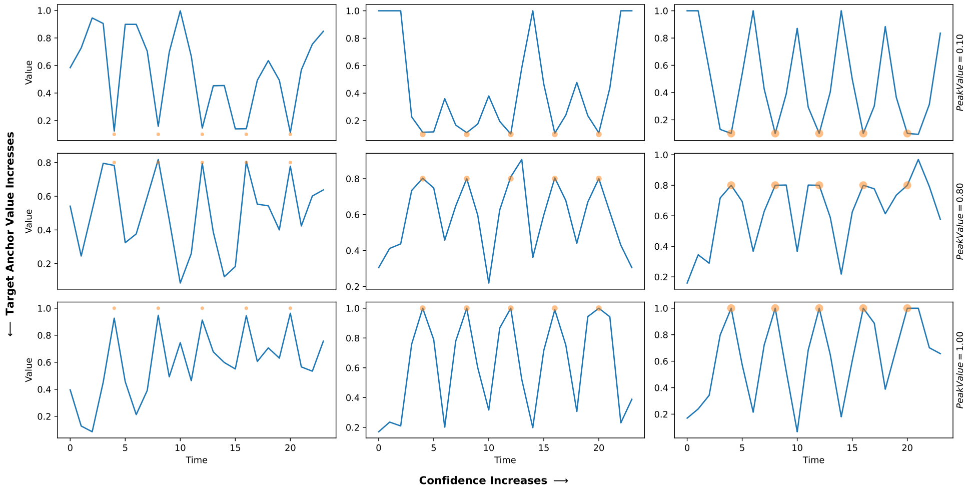

Figure 11. Demonstration of Anchor Control in fMRI datasets with multiple anchor points and confidences.

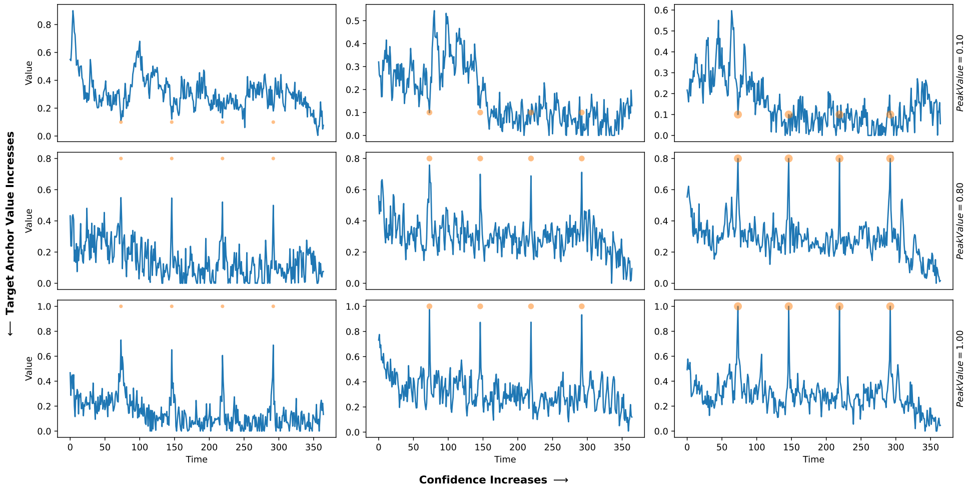

Figure 12. Demonstration of Anchor Control in Revenue datasets with multiple anchor points and confidences

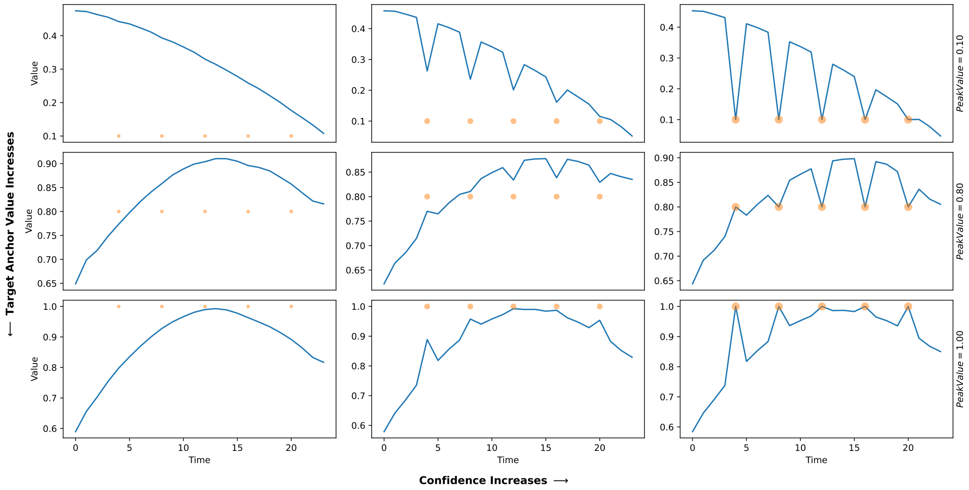

Figure 13. Demonstration of Anchor Control in Synthetic sine wave datasets with multiple anchor points and confidences

C.1.3. Float Mask Control with Extensions (CSDI)

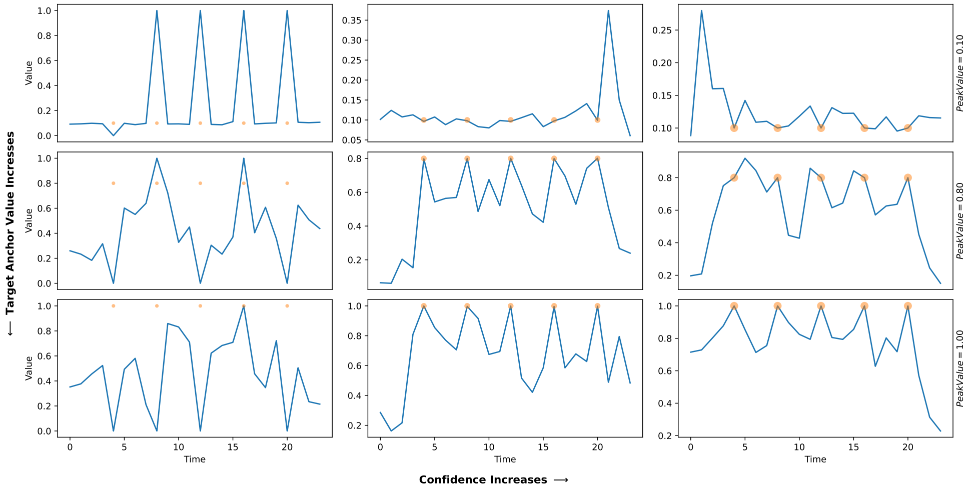

Figure 14. Demonstration of Anchor Control in ETTh datasets with multiple anchor points and confidences

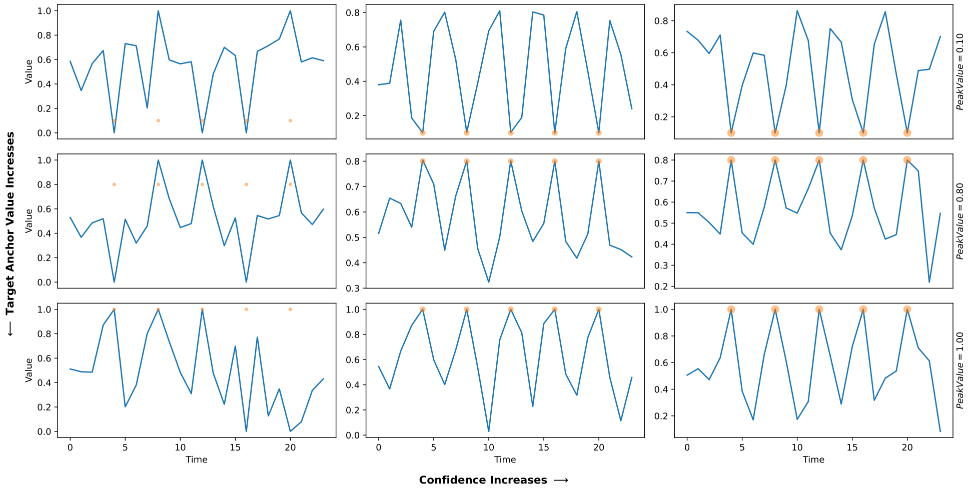

Figure 15. Demonstration of Anchor Control in fMRI datasets with multiple anchor points and confidences.

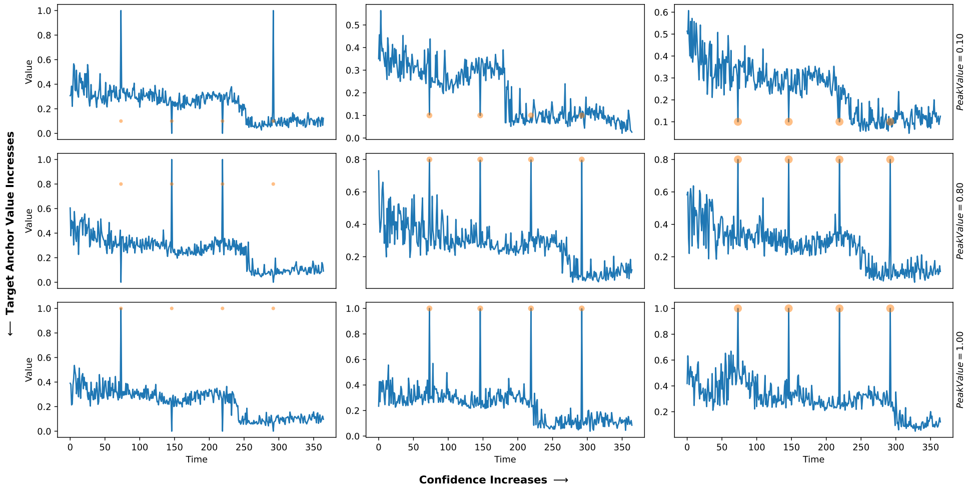

Figure 16. Demonstration of Anchor Control in Revenue datasets with multiple anchor points and confidences

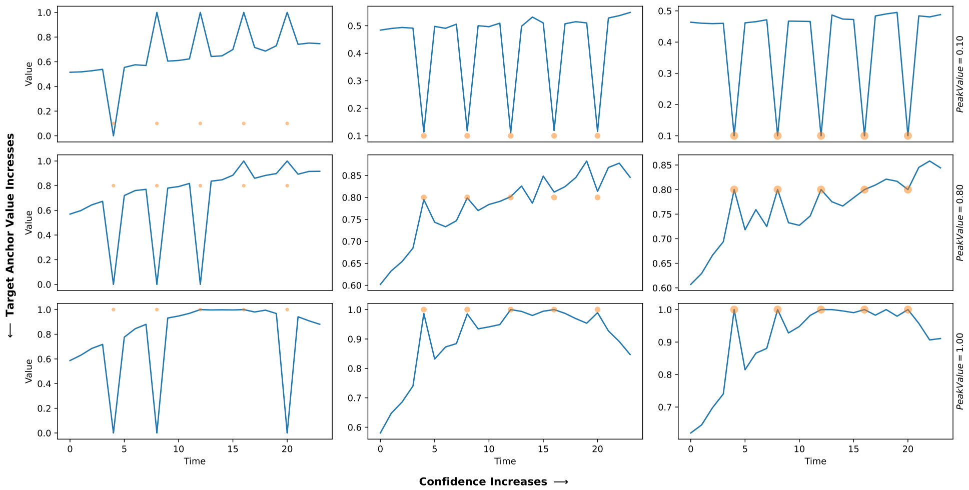

Figure 17. Demonstration of Anchor Control in Synthetic sine wave datasets with multiple anchor points and confidences

C.2. KED of Anchor Control

The following plots of Kernel Density Estimation (KDE) clearly demonstrate how the distribution peaks (purple dash line) shift towards the anchor points as confidence increases. For instance, in the ETTh dataset, the most pronounced shift occurs at anchor points under the highest confidence level. The model generates sequences that accurately respect anchor points while preserving the dataset's inherent distributional characteristics. In Figure C.2.3's middle row, where the target value is 0.8, increasing confidence levels cause the peaks (y-value density) of controlled results (purple line) to intensify and converge toward the target value. This pattern is consistently observed across all datasets.

C.2.1. Pure Float Mask Control (Diffusion-TS)

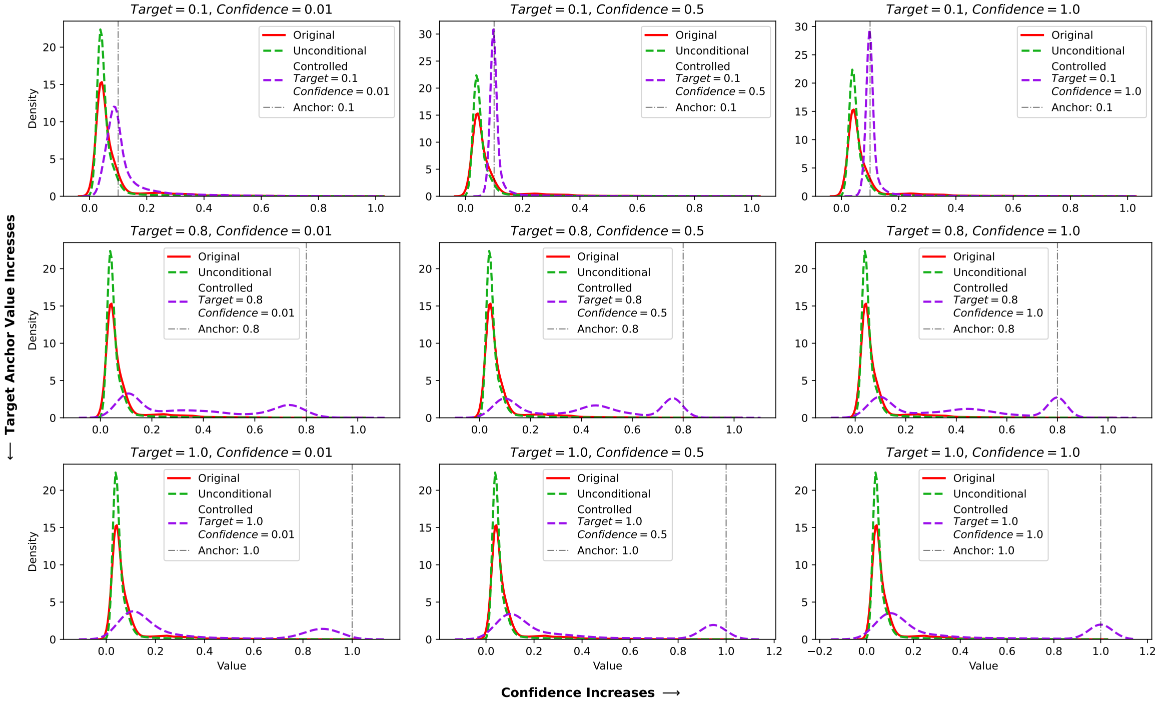

Figure 18. KDE analysis of ETTh dataset generation with anchor points.

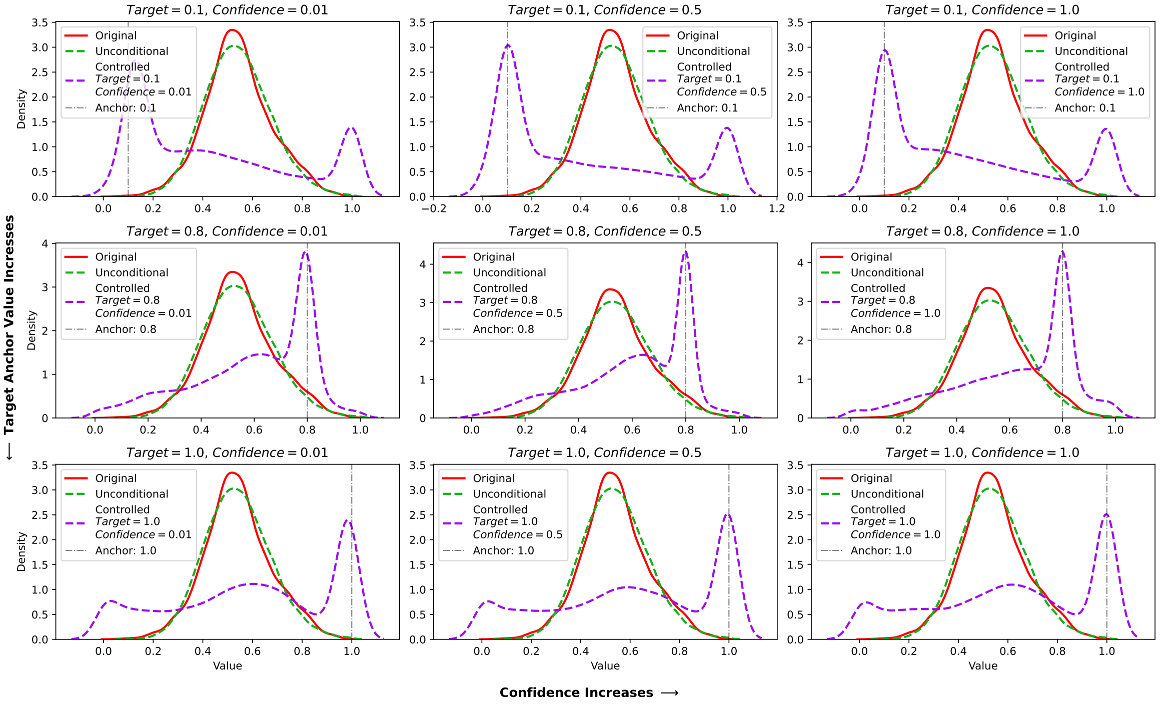

Figure 19. KDE analysis of fMRI dataset generation with anchor points.

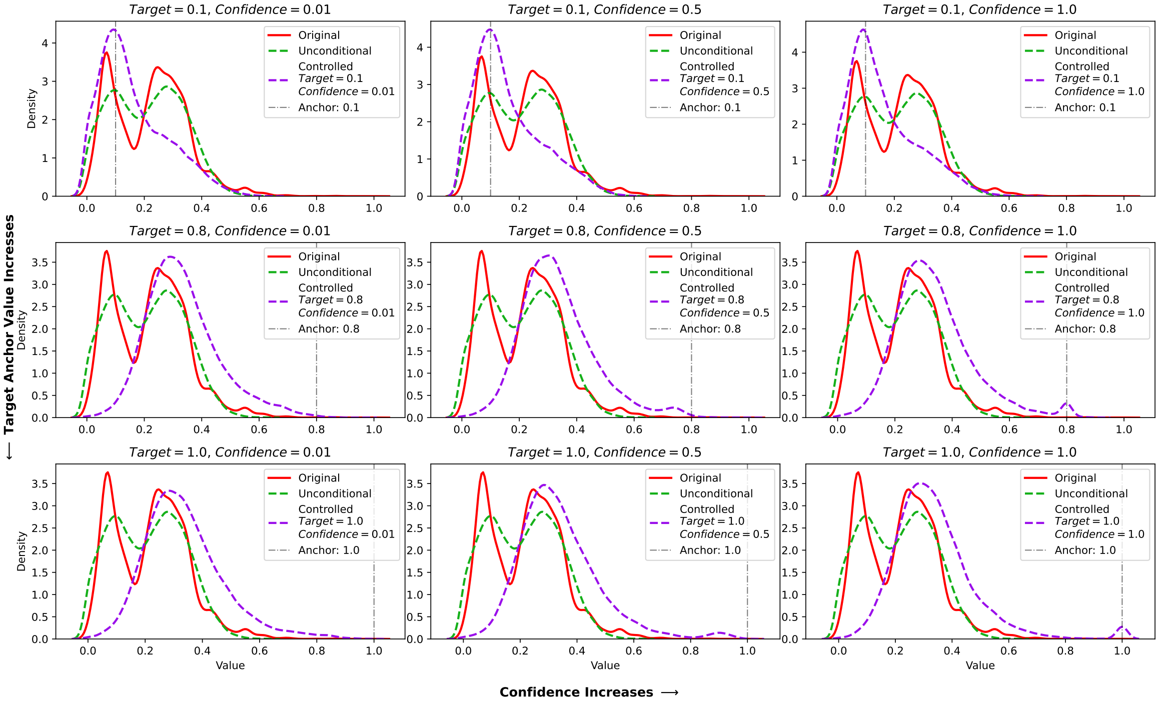

Figure 20. KDE analysis of Revenue dataset generation with anchor points.

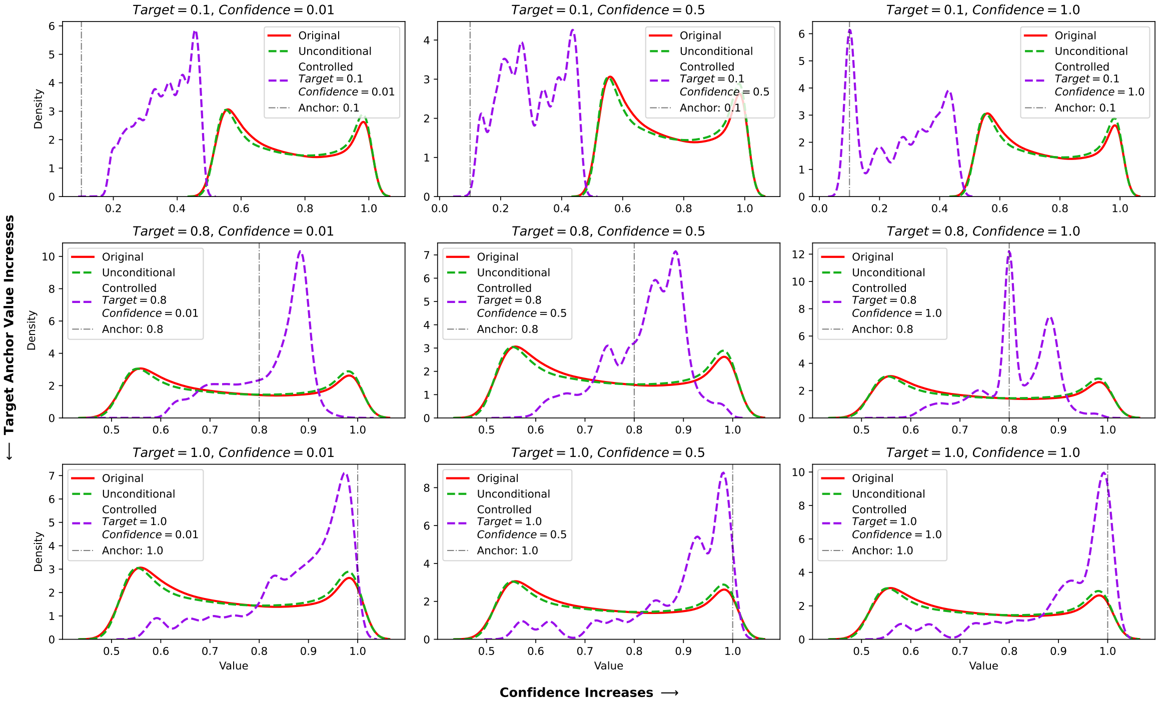

Figure 21. KDE analysis of synthetic sine wave dataset generation with anchor points.

C.2.2. Float Mask Control with Extensions (Diffusion-TS)

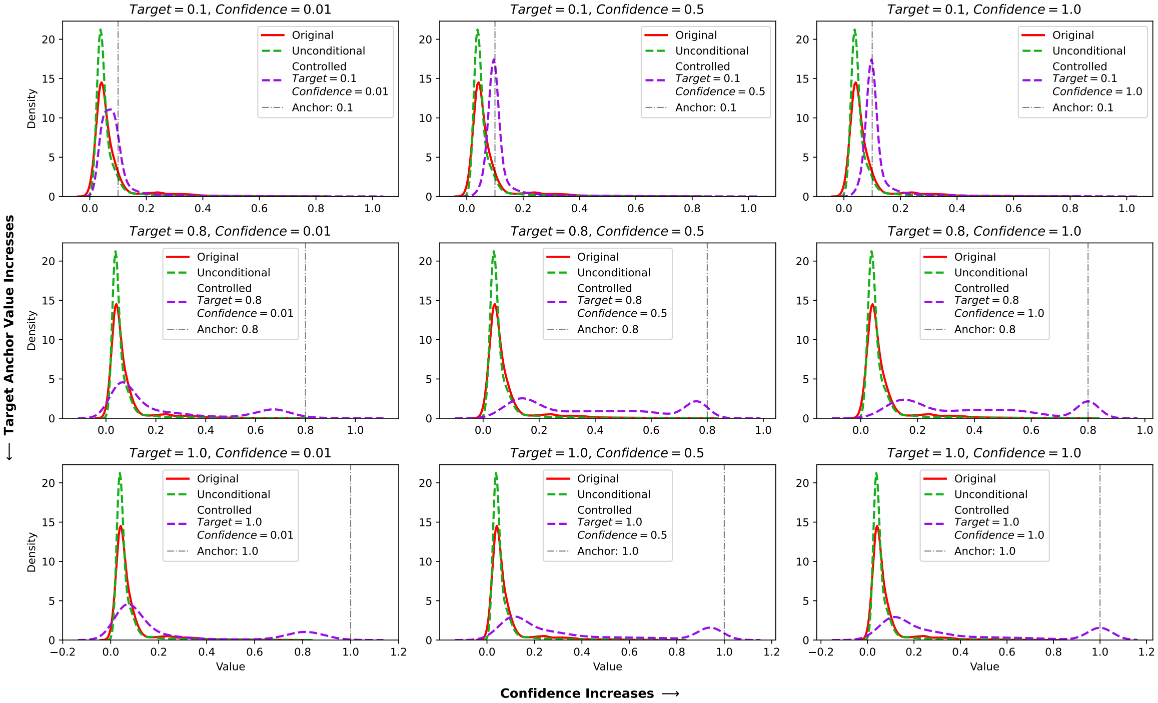

Figure 22. KDE analysis of ETTh dataset generation with anchor points.

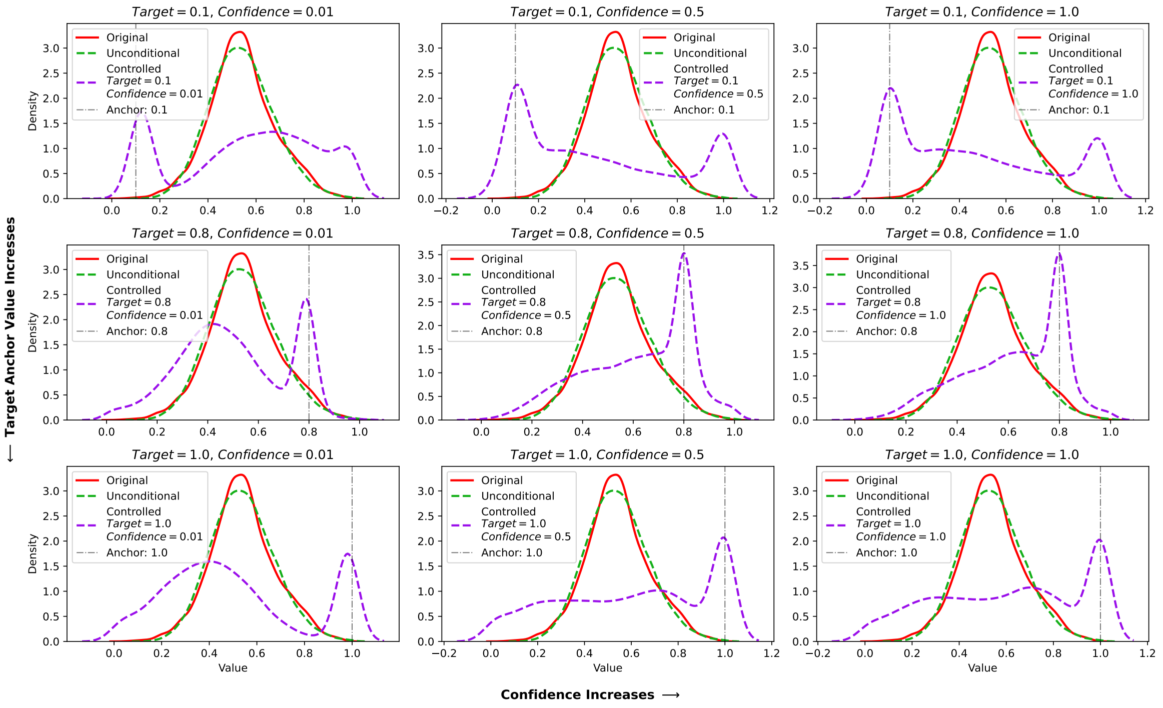

Figure 23. KDE analysis of fMRI dataset generation with anchor points.

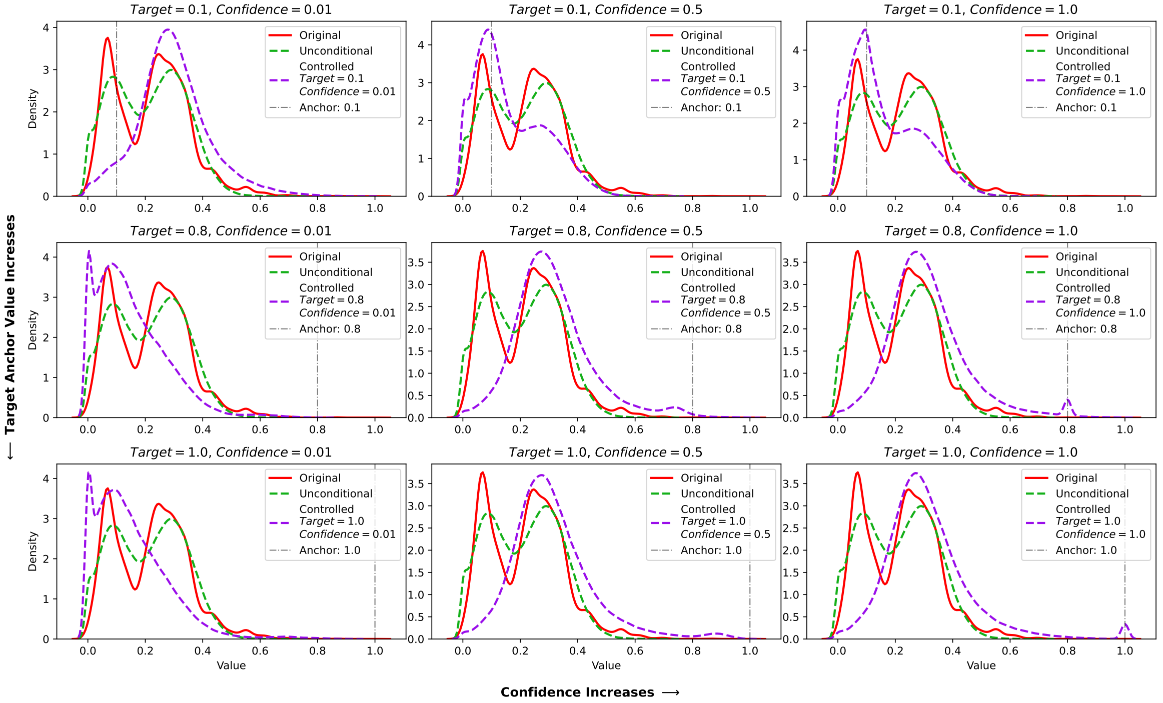

Figure 24. KDE analysis of Revenue dataset generation with anchor points.

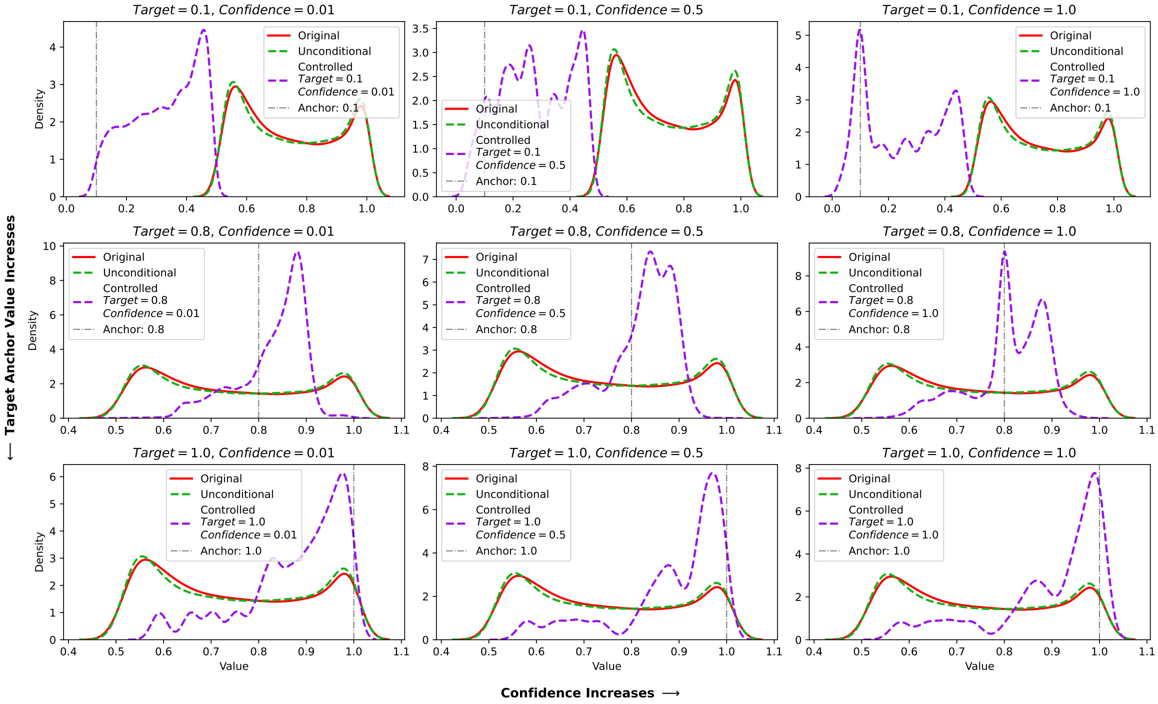

Figure 25. KDE analysis of synthetic sine wave dataset generation with anchor points.

C.2.3. Float Mask Control with Extensions (CSDI)

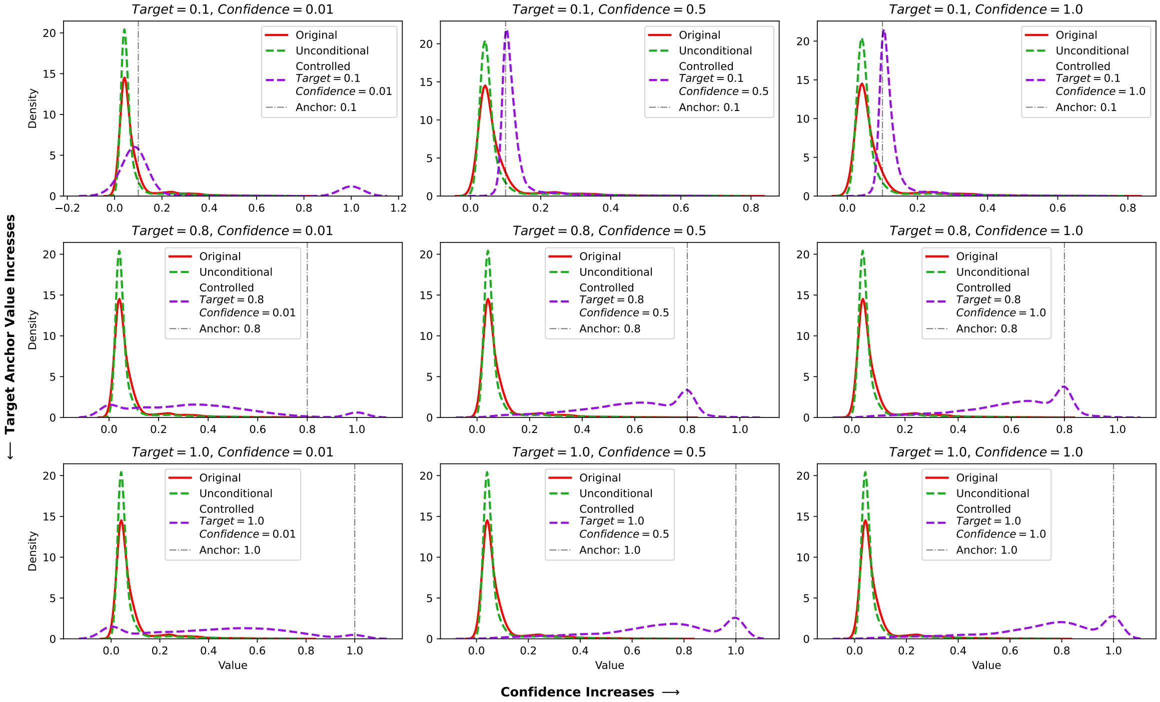

Figure 26. KDE analysis of ETTh dataset generation with anchor points.

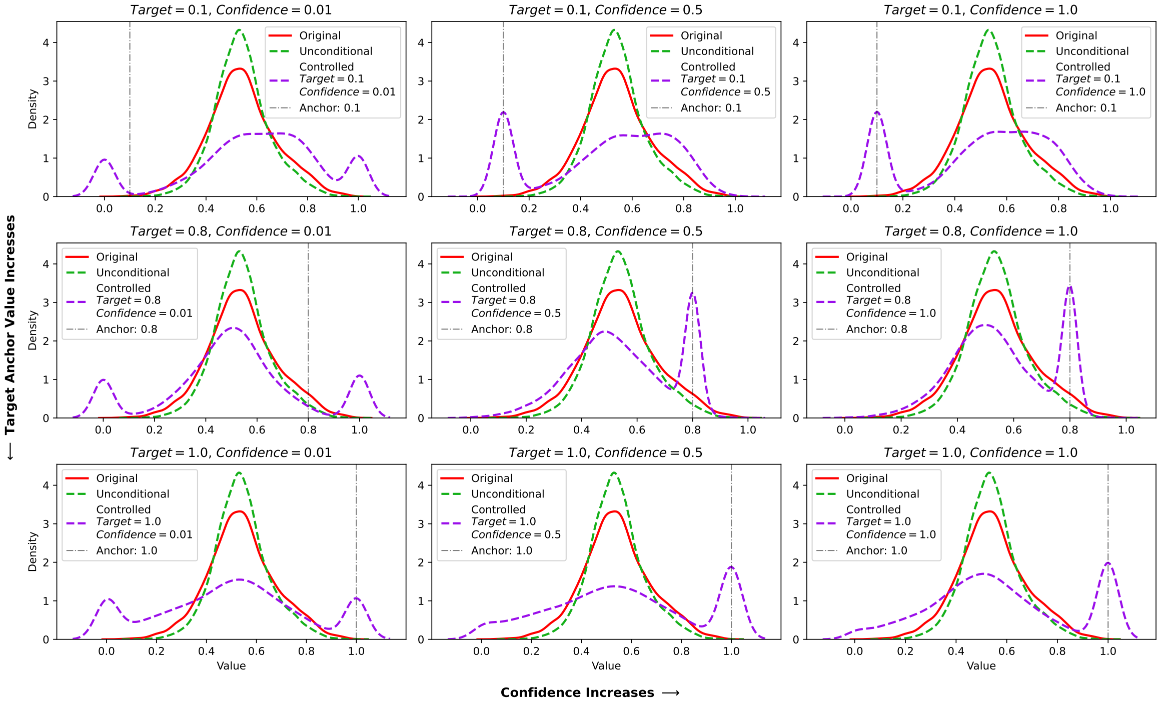

Figure 27. KDE analysis of fMRI dataset generation with anchor points.

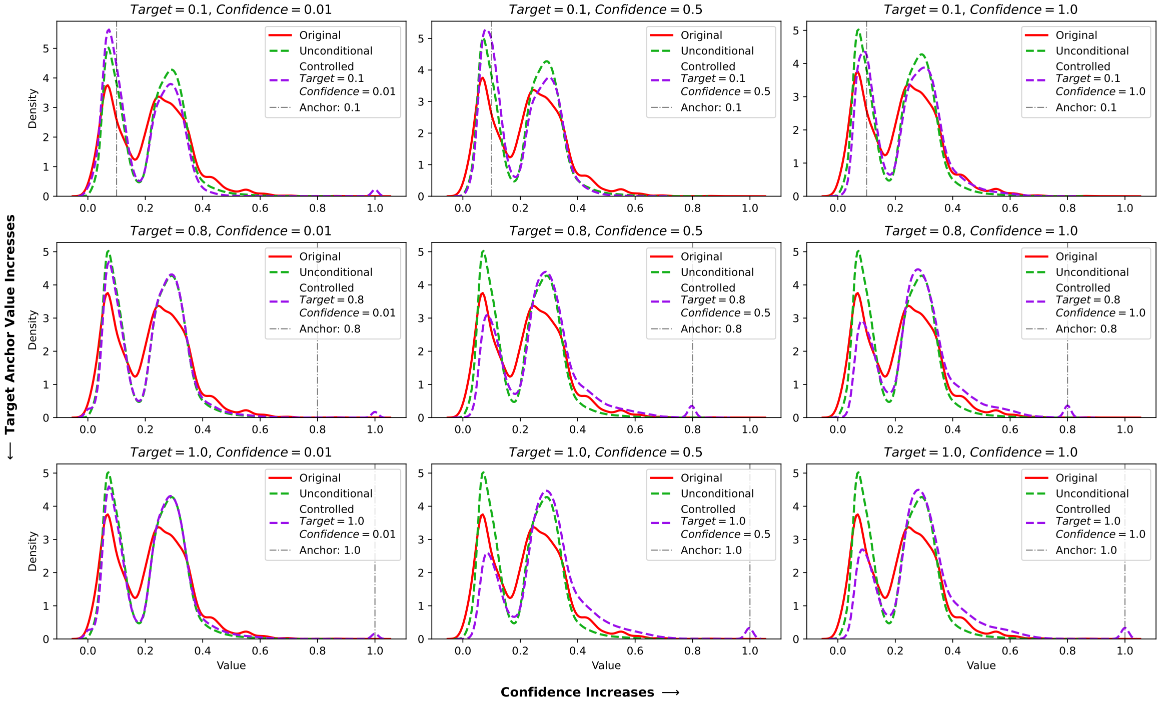

Figure 28. KDE analysis of Revenue dataset generation with anchor points.

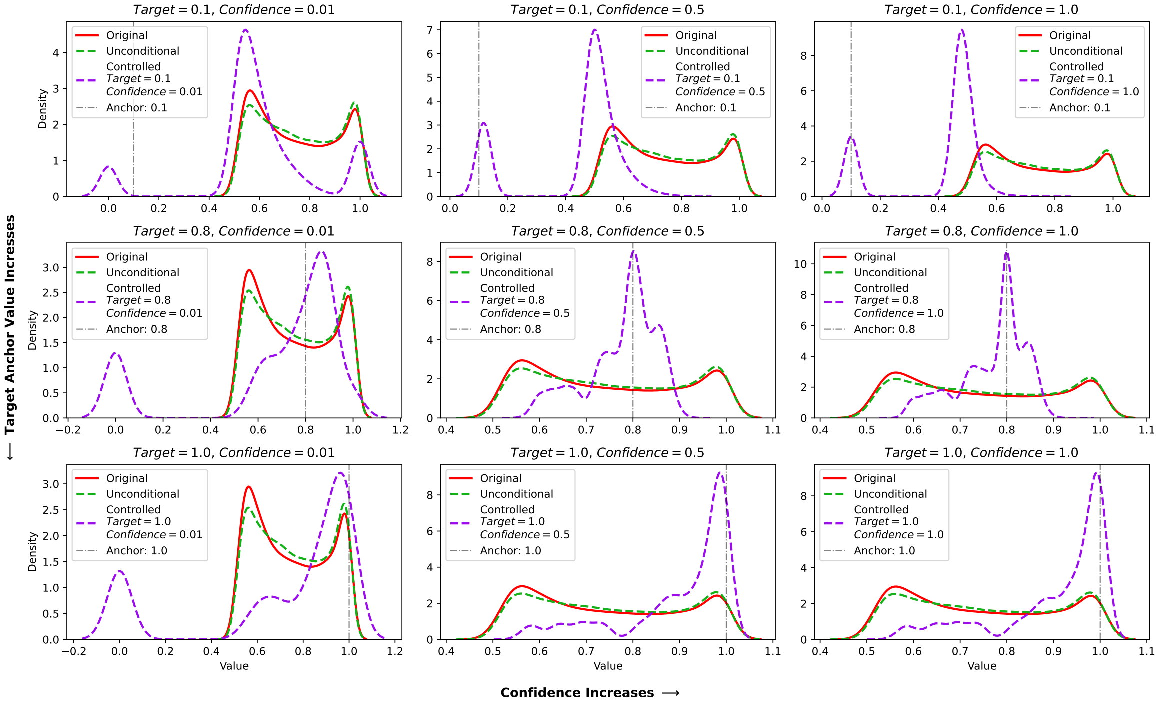

Figure 29. KDE analysis of synthetic sine wave dataset generation with anchor points.

C.3. Supplement Metrics

The Discriminative, Predictive, Context-FID, and Correlational scores help quantify distribution shifts under anchor control. Table C.3 demonstrates that all metrics increase significantly after applying control, indicating that the control signals effectively influence the generated time series. But our method makes them more distinguishable from the original distribution, which is the improved direction for following research.

Table 9. Supplemental metrics for anchor control performance across different datasets and target values. The results show discriminative, predictive, context-FID, and correlational scores for each dataset and control configuration. Lower scores indicate better performance.

Metrics	Control Signal	Dataset			
		ETTh	Revenue	fMRI	Sine
Discriminative Score (Lower is Better)	Unconditional	0.103±0.042	0.082±0.093	0.141±0.037	0.031±0.023
	Confidence=0.01	0.497±0.005	0.382±0.267	0.500±0.000	0.457±0.027
	Confidence=0.5	0.496±0.006	0.282±0.323	0.499±0.001	0.494±0.004
	Confidence=1.0	0.498±0.001	0.009±0.025	0.498±0.000	0.374±0.264
Predictive Score (Lower is Better)	Unconditional	0.256±0.002	0.065±0.026	0.103±0.002	0.094±0.000
	Confidence=0.01	0.302±0.008	0.181±0.002	0.134±0.010	0.120±0.007
	Confidence=0.5	0.305±0.014	0.179±0.005	0.141±0.010	0.118±0.012
	Confidence=1.0	0.335±0.019	0.175±0.009	0.139±0.009	0.116±0.008
Context-FID Score (Lower is Better)	Unconditional	0.108±0.007	1.230±0.284	0.260±0.024	0.034±0.005
	Confidence=0.01	7.797±0.644	4.654±1.389	15.671±2.920	4.169±1.139
	Confidence=0.5	6.973±1.514	5.921±0.711	15.463±1.888	10.842±2.103
	Confidence=1.0	7.856±1.326	7.083±0.512	13.854±0.830	8.906±1.168
Correlational Score (Lower is Better)	Unconditional	2.313±0.743	0.038±0.013	2.672±0.091	0.066±0.009
	Confidence=0.01	9.321±0.764	0.122±0.007	16.699±0.453	0.255±0.013
	Confidence=0.5	8.445±0.675	0.119±0.006	15.488±0.174	0.468±0.016
	Confidence=1.0	9.640±0.835	0.121±0.011	17.259±0.434	0.345±0.034

C.4. Anchor Control Analysis

Here, we demonstrate again the complete aggregated Mean Absolute Deviation (MAD) of anchor control across all datasets, providing solid evidence for the effectiveness of anchor control in maintaining anchor points.

C.4.1. Pure Float Mask Control

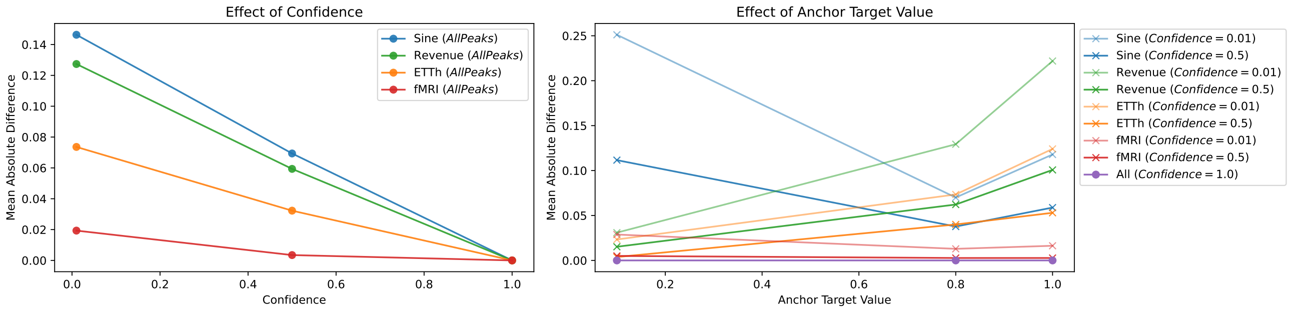

Figure 30. Different combinations of confidence levels and target values across all datasets. (Diffusion-TS)

C.4.2. Float Mask Control with Extensions

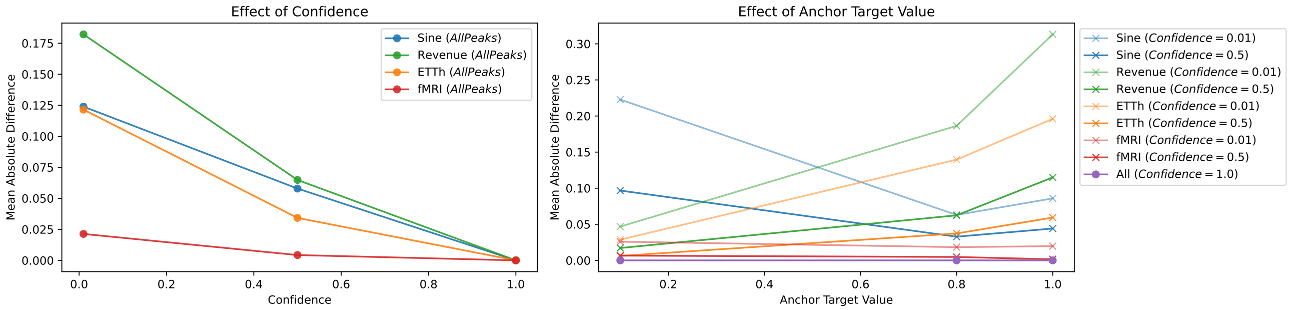

Figure 31. Different combinations of confidence levels and target values cross all datasets. (Diffusion-TS)

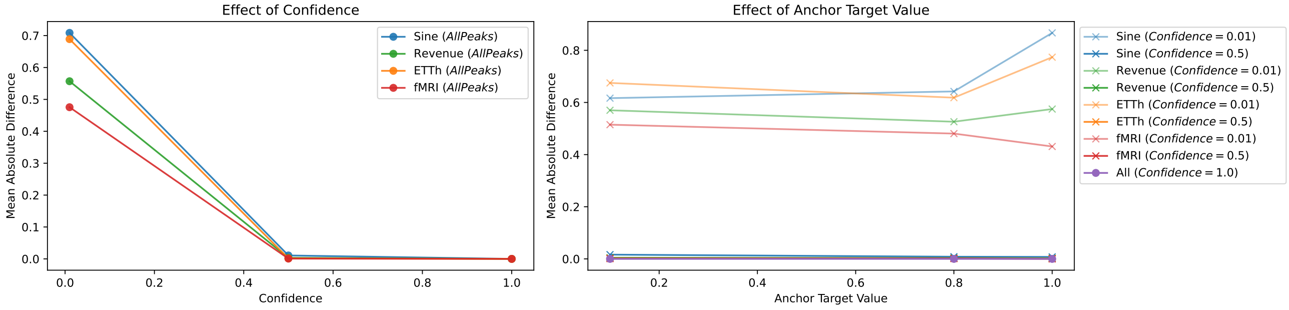

Figure 32. Different combinations of confidence levels and target values across all datasets. (CDSI)

D. Statistic Control

This section provides supplementary materials for analyzing statistical control, focusing on both Sum Control and Segment-Wise Sum Control.

D.1. Demonstration

The following figures demonstrate the effectiveness of sum control across different datasets. As the target value increases (from left to right in each row), the model generates sequences that successfully adhere to the sum constraints while maintaining the dataset's inherent distributional properties. For segment-wise sum control, the results consistently show that the model tends to increase the overall sequence sum value, which aligns with the objective of preserving the original distribution learned from the dataset.

D.1.1. Whole Time Series Summation Control (Diffusion-TS)

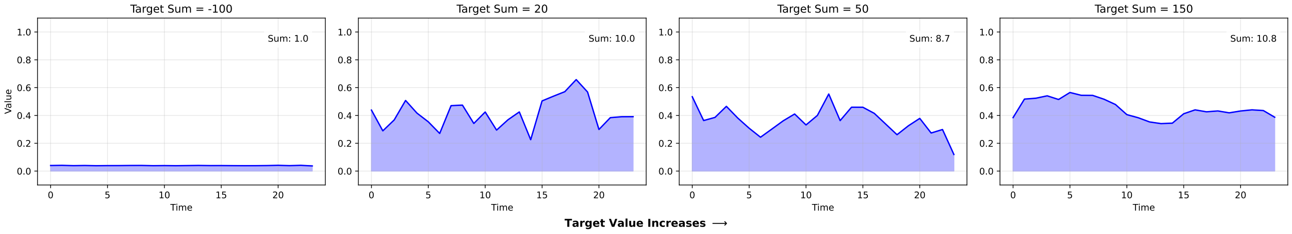

Figure 33. Demonstration of Sum Control on ETTh dataset.

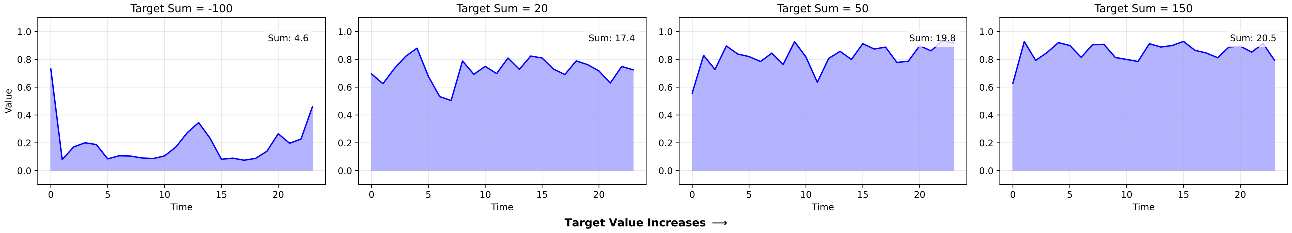

Figure 34. Demonstration of Sum Control on fMRI dataset.

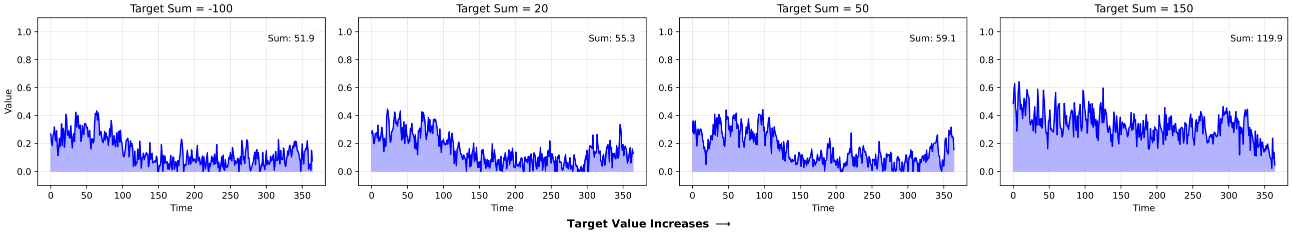

Figure 35. Demonstration of Sum Control on Revenue dataset.

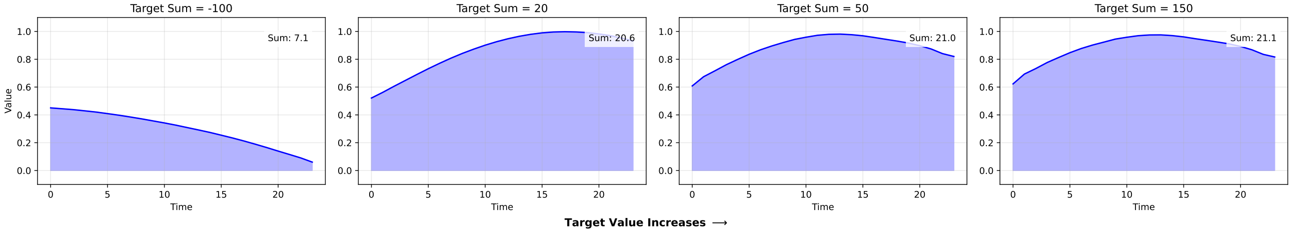

Figure 36. Demonstration of Sum Control on synthetic sine wave dataset.

D.1.2. Whole Time Series Summation Control (CSDI)

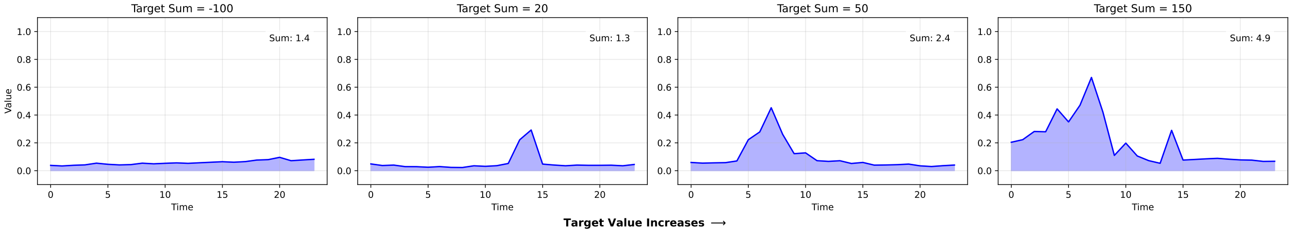

Figure 37. Demonstration of Sum Control on ETTh dataset.

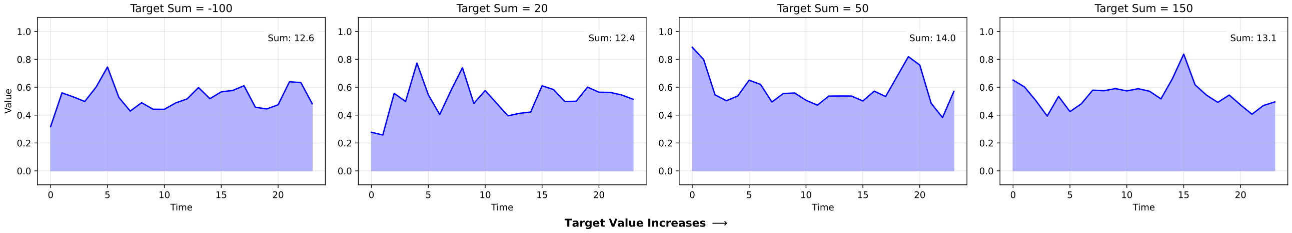

Figure 38. Demonstration of Sum Control on fMRI dataset.

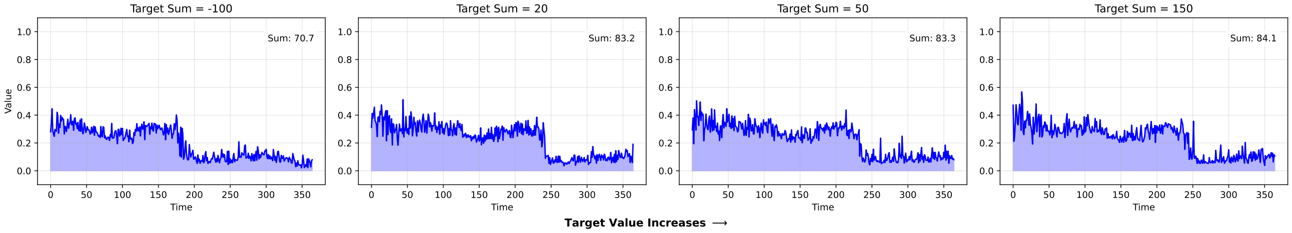

Figure 39. Demonstration of Sum Control on Revenue dataset.

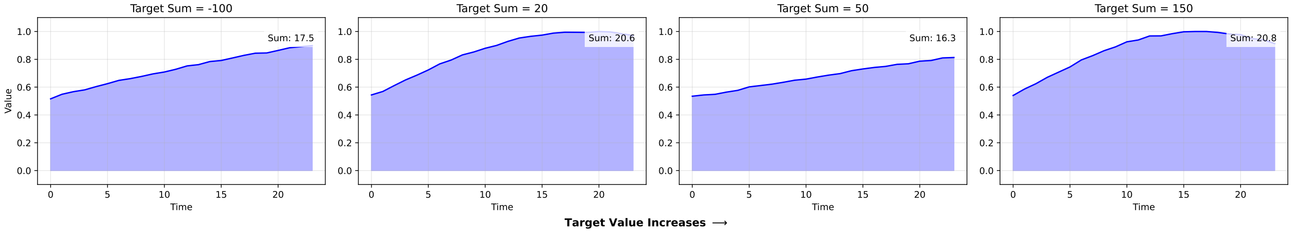

Figure 40. Demonstration of Sum Control on synthetic sine wave dataset.

D.1.3. Segment Wise Sum Control (Diffusion-TS)

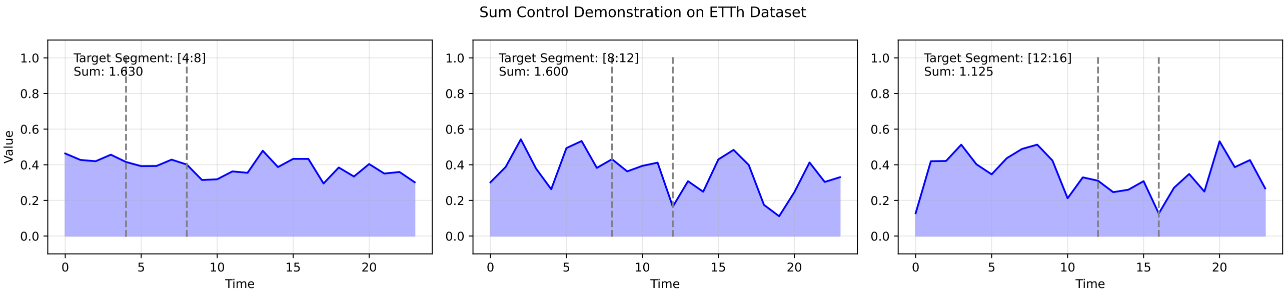

Figure 41. Demonstration of Segment-Wise Sum Control on ETTh dataset.

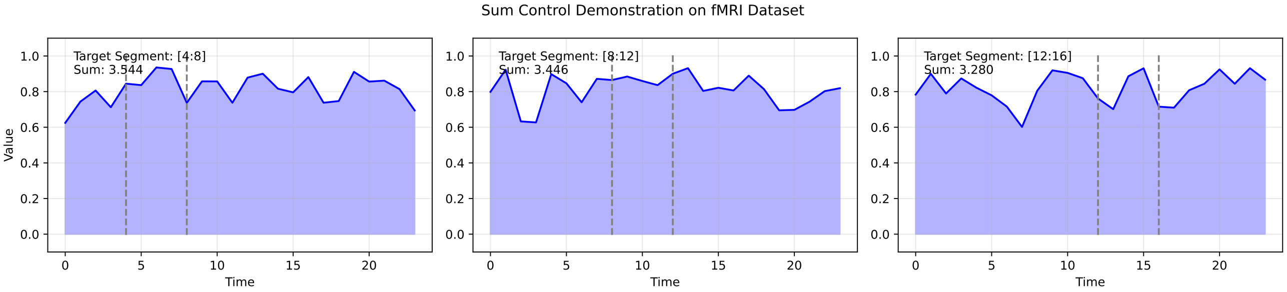

Figure 42. Demonstration of Segment-Wise Sum Control on fMRI dataset.

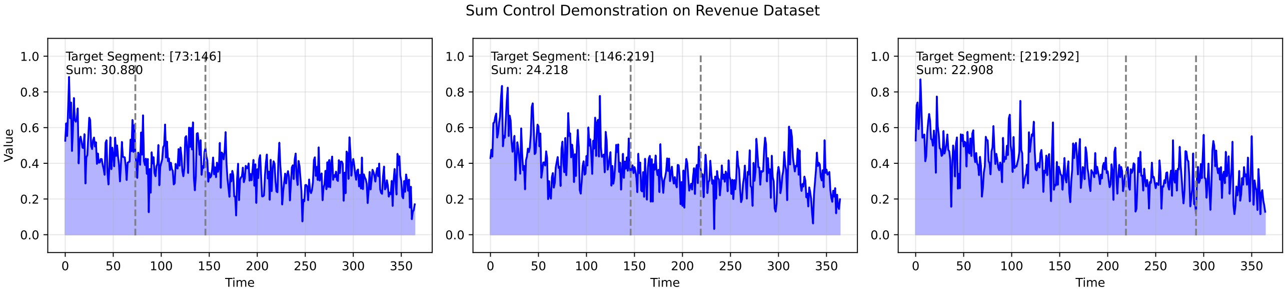

Figure 43. Demonstration of Segment-Wise Sum Control on Revenue dataset.

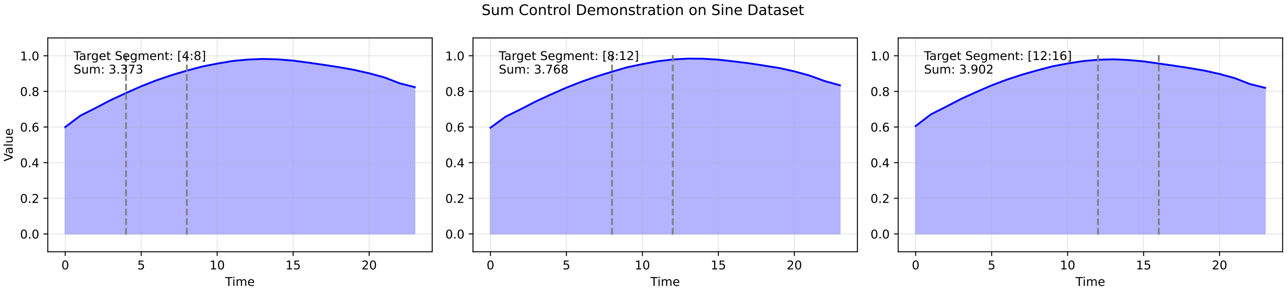

Figure 44. Demonstration of Segment-Wise Sum Control on synthetic sine wave dataset.

D.1.4. Segment Wise Sum Control (CSDI)

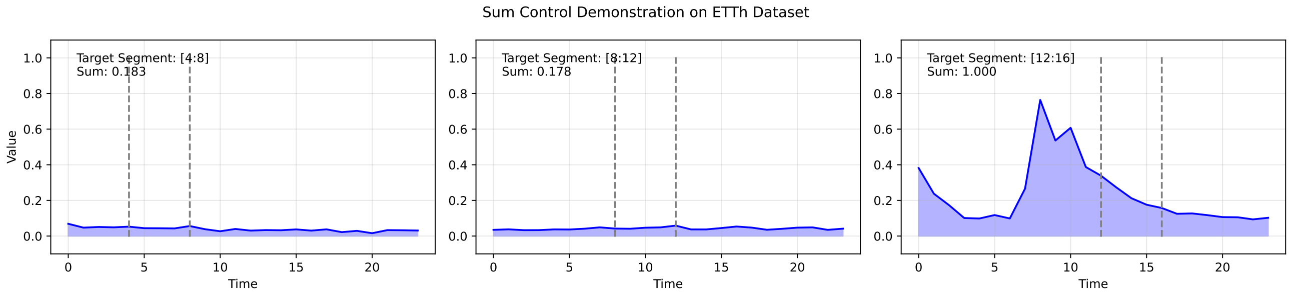

Figure 45. Demonstration of Segment-Wise Sum Control on ETTh dataset.

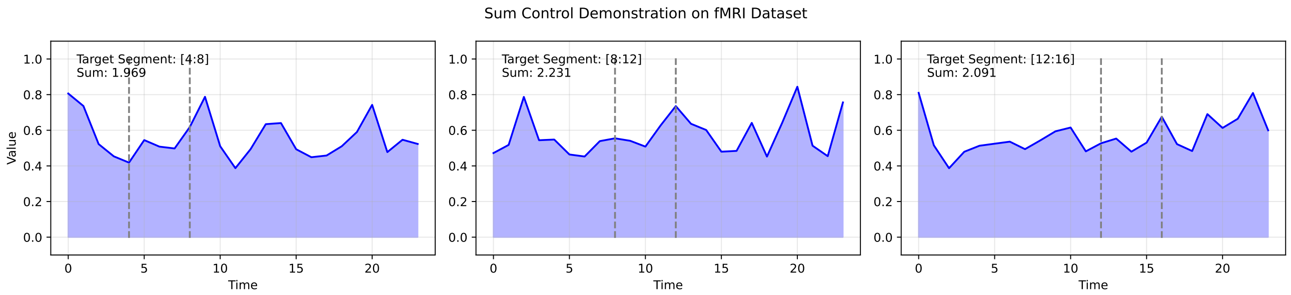

Figure 46. Demonstration of Segment-Wise Sum Control on fMRI dataset.

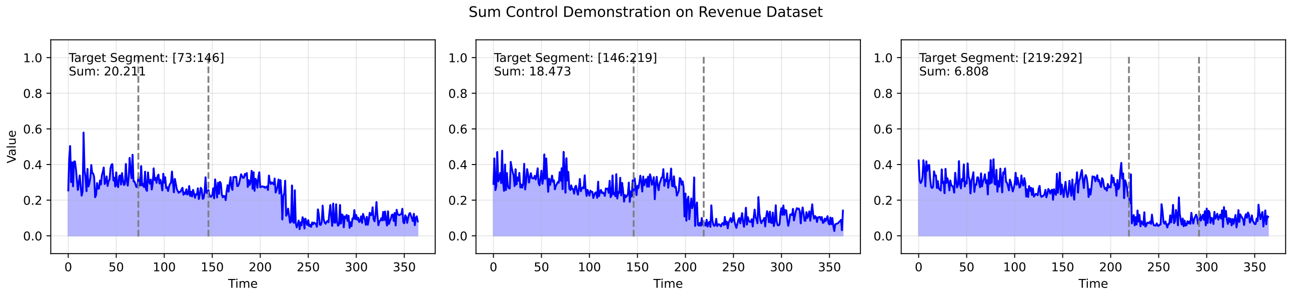

Figure 47. Demonstration of Segment-Wise Sum Control on Revenue dataset.

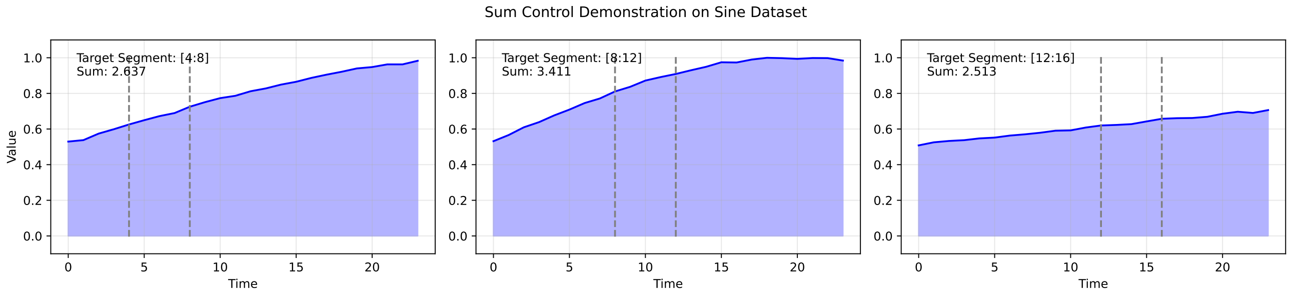

Figure 48. Demonstration of Segment-Wise Sum Control on synthetic sine wave dataset.

D.2. Kernel Density Estimate of Sum Control

Similar to the KDE analysis of anchor control, we present KDE analysis for sum control across different datasets. The KDE peaks of controlled output (purple line) shift rightward compared to original and unconditional distributions, confirming that controlled sequences achieve higher sum values while preserving dataset-specific distributional characteristics. While this pattern does not persist consistently across different control weights and need to be further investigated.

D.2.1. KDE of Total Sum Control (Diffusion-TS)

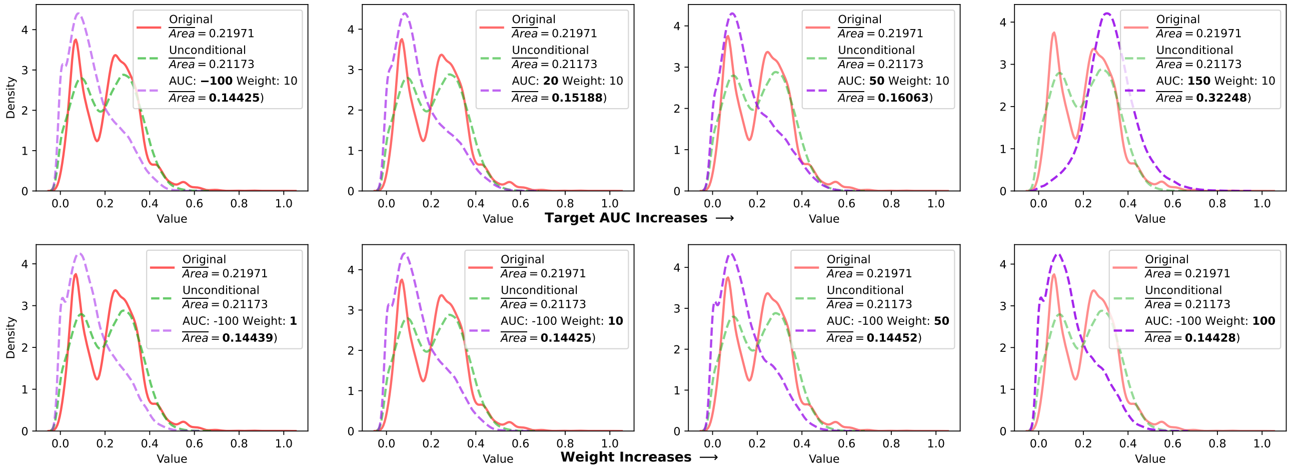

Figure 49. Kernel density estimation analysis of Revenue dataset under varying sum control targets. Top: Target analysis showing control effectiveness. Bottom: Weight analysis showing control effectiveness.

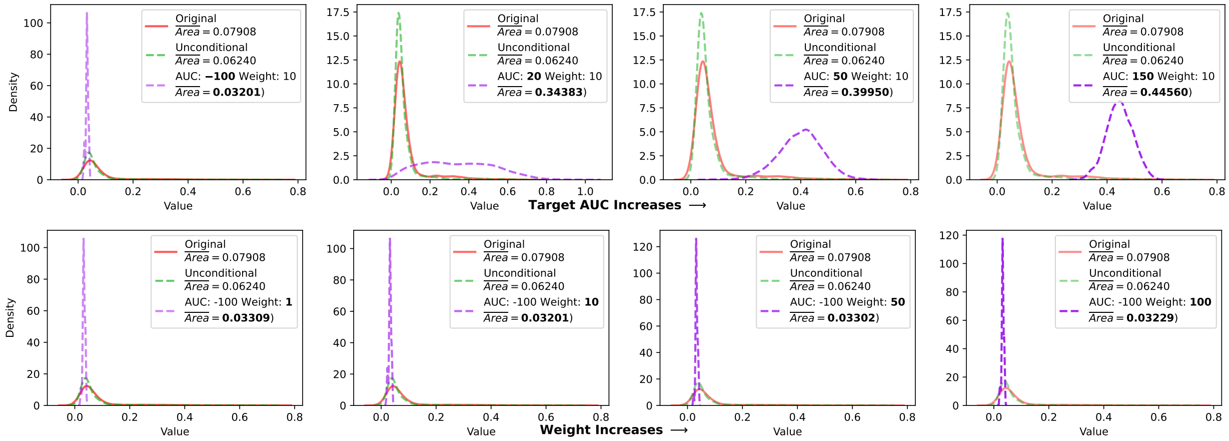

Figure 50. Kernel density estimation visualization for ETTh dataset. Top: Sum control analysis. Bottom: Weight analysis.

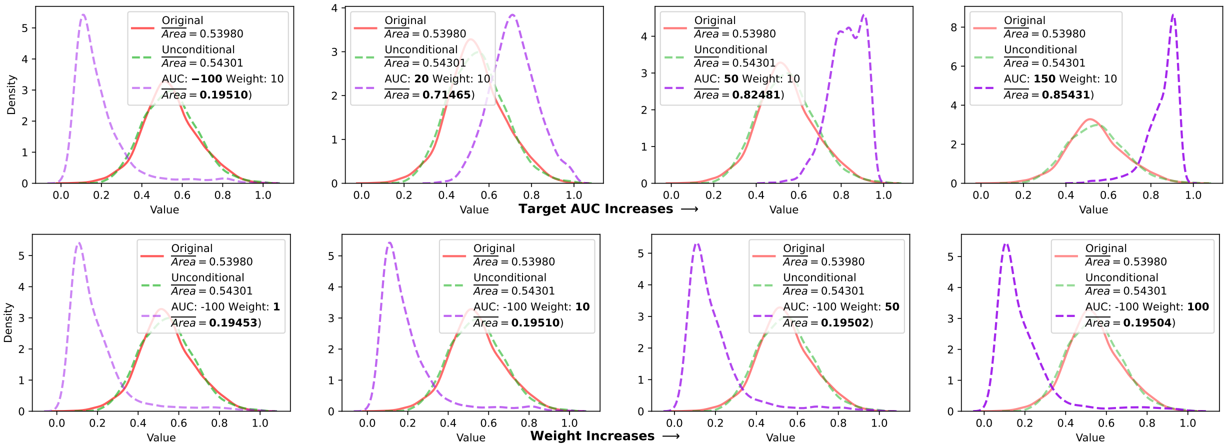

Figure 51. Kernel density estimation analysis of fMRI dataset. Top: Sum control analysis. Bottom: Weight analysis.

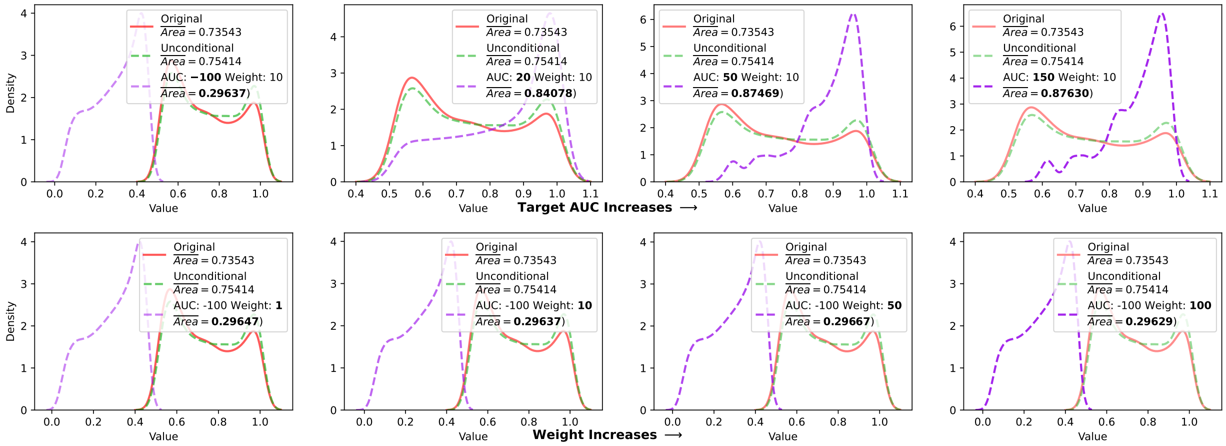

Figure 52. Kernel density estimation analysis of synthetic sine wave dataset. Top: Sum control analysis. Bottom: Weight analysis.

D.2.2. KDE of Total Sum Control (CSDI)

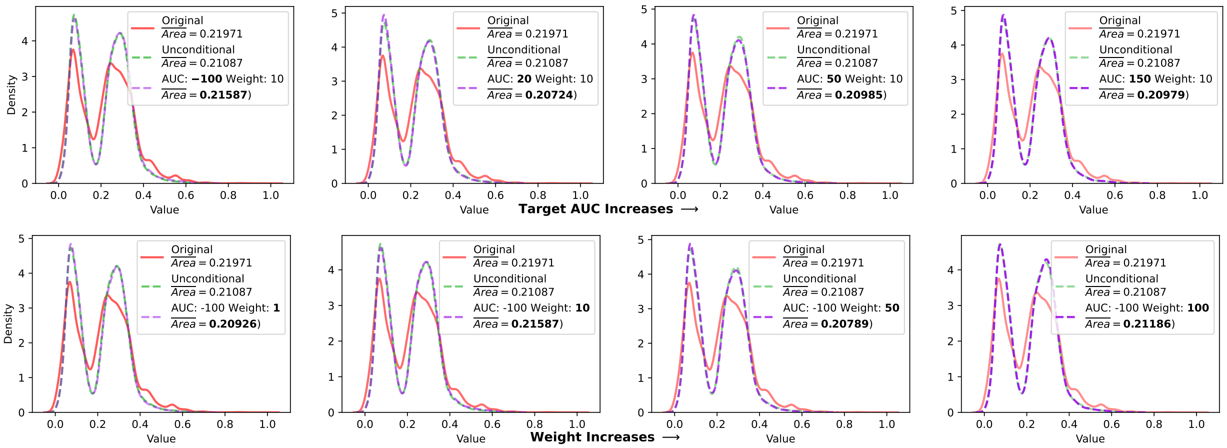

Figure 53. Kernel density estimation analysis of Revenue dataset under varying sum control targets. Top: Target analysis showing control effectiveness. Bottom: Weight analysis showing control effectiveness.

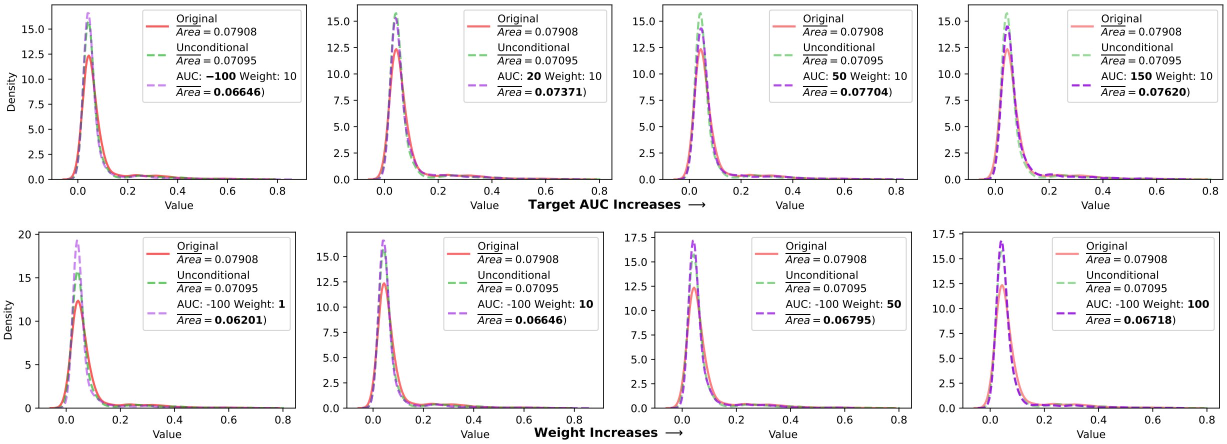

Figure 54. Kernel density estimation visualization for ETTh dataset. Top: Sum control analysis. Bottom: Weight analysis.

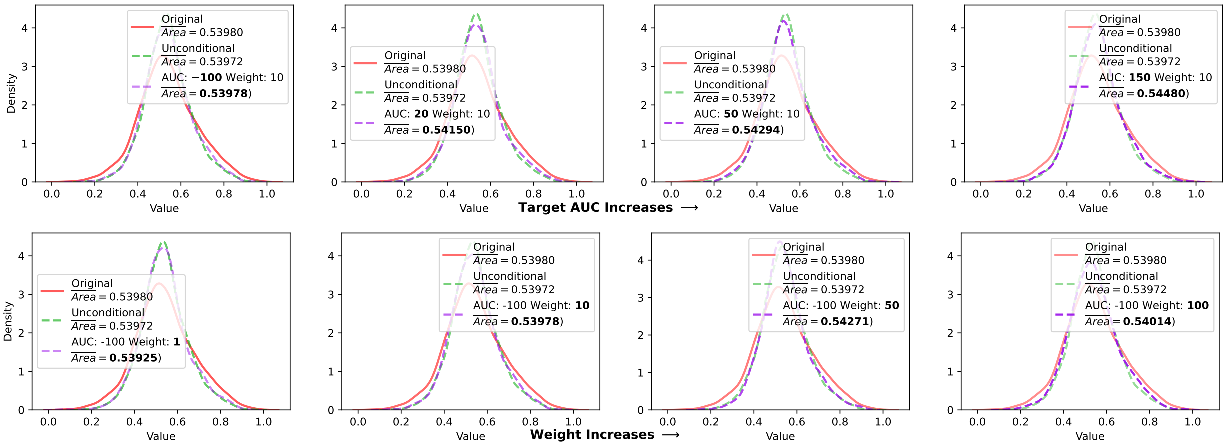

Figure 55. Kernel density estimation analysis of fMRI dataset. Top: Sum control analysis. Bottom: Weight analysis.

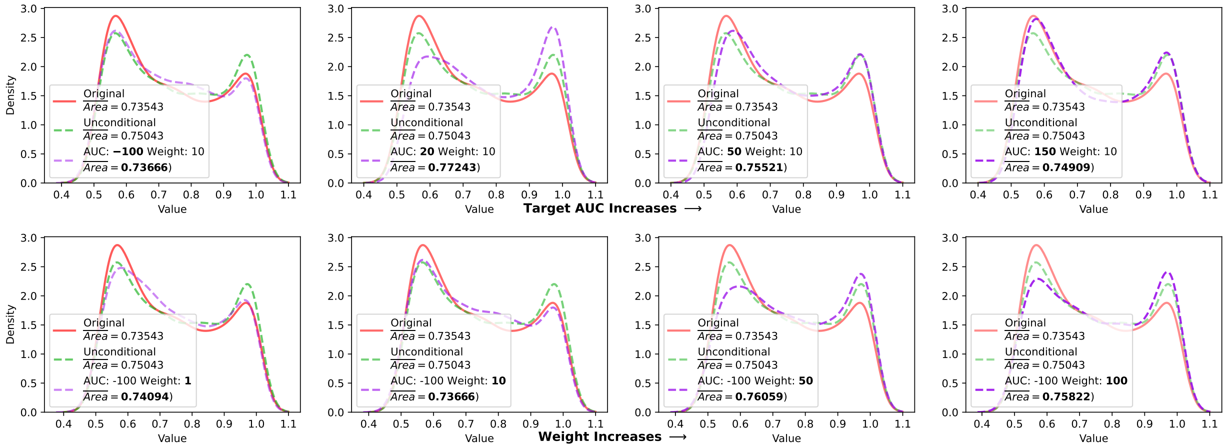

Figure 56. Kernel density estimation analysis of synthetic sine wave dataset. Top: Sum control analysis. Bottom: Weight analysis.

D.3. Averaged Sum Change Over All Segments

For the following aggregated sum change over all segments, we calculate the averaged value over segments for each dataset, with a target sum value of 150 for each segment.

D.3.1. Value Change of Segment Sum Control (Diffusion-TS)

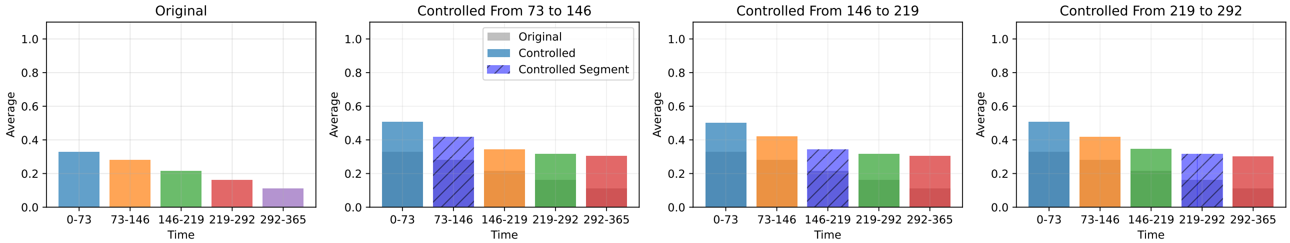

Figure 57. Segmented Summation Control on Revenue dataset.

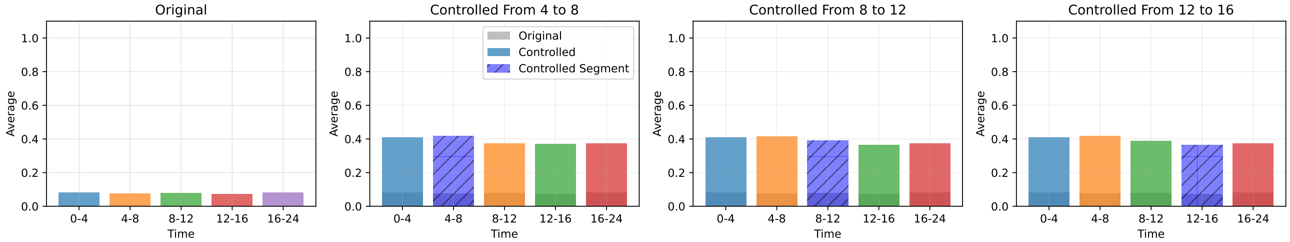

Figure 58. Segmented Summation Control on ETTh dataset.

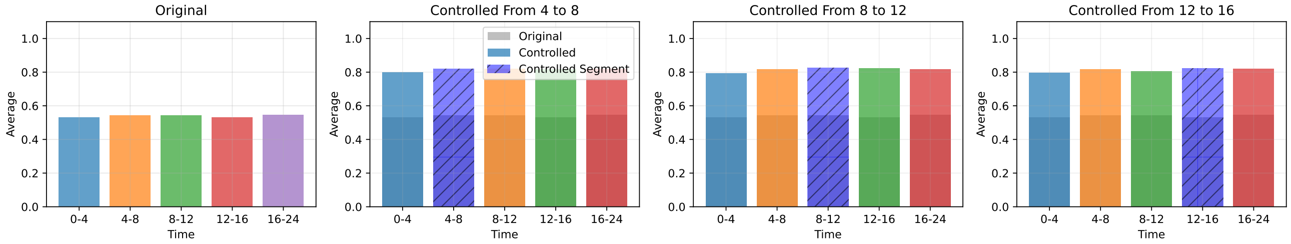

Figure 59. Segmented Summation Control on fMRI dataset.

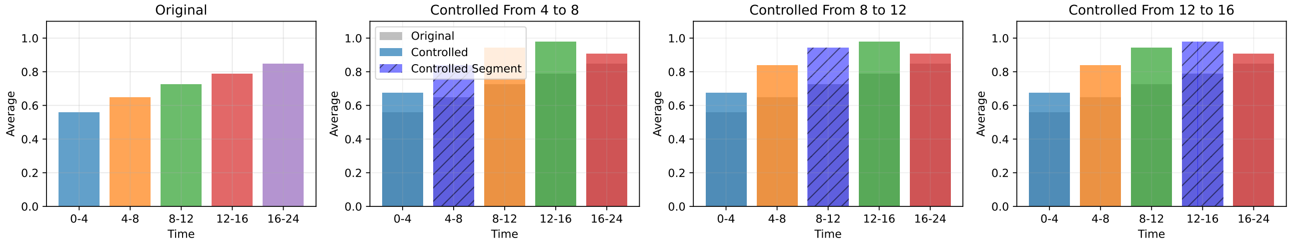

Figure 60. Segmented Summation Control on Sine dataset.

D.3.2. Value Change of Segment Sum Control (CSDI)

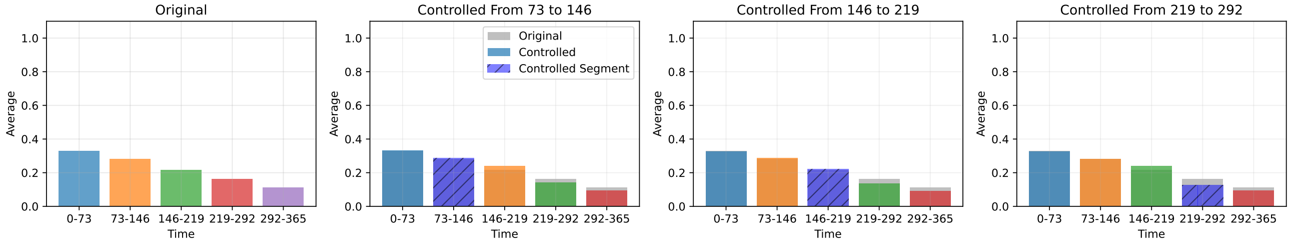

Figure 61. Segmented Summation Control on Revenue dataset.

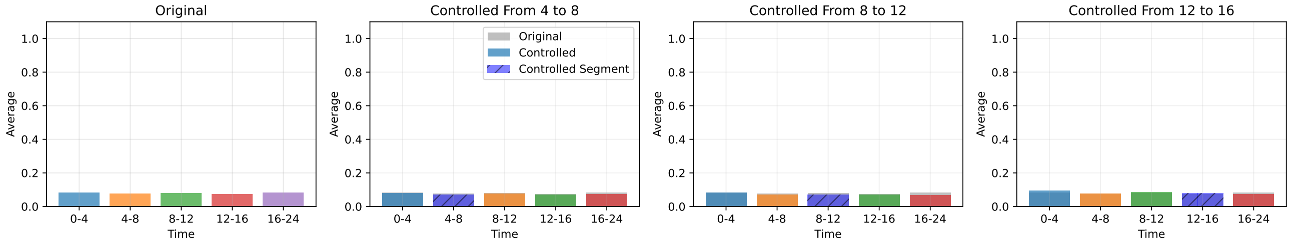

Figure 62. Segmented Summation Control on ETTh dataset.

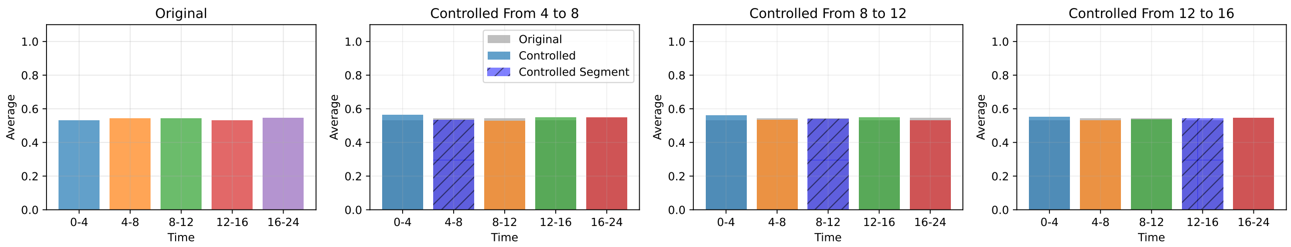

Figure 63. Segmented Summation Control on fMRI dataset.

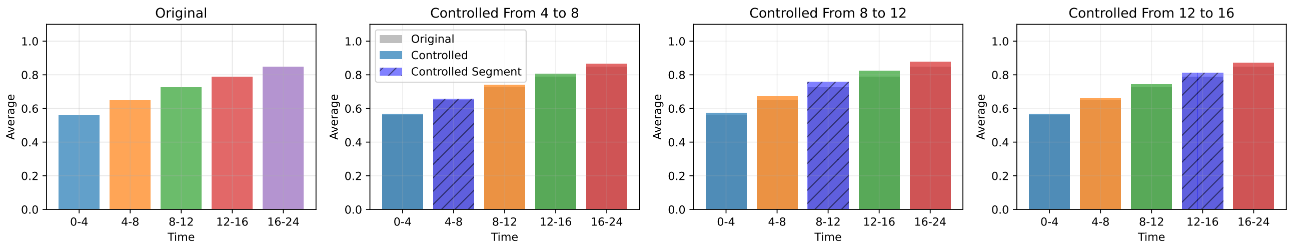

Figure 64. Segmented Summation Control on Sine dataset.

D.4. Supplement Metrics

The Discriminative, Predictive, Context-FID, and Correlational scores help quantify distribution shifts under sum control. Table D.4 demonstrates that all metrics increase significantly after applying control, indicating that the control signals effectively influence the generated time series and make them more distinguishable from the original distribution.

Table 10. Supplemental metrics for sum control performance across different datasets and target values. The results show discriminative, predictive, context-FID, and correlational scores for each dataset and control configuration. Lower scores indicate better performance.

Metrics	Control Signal	Dataset			
		ETTh	Revenue	fMRI	Sine
Discriminative Score (Lower is Better)	Unconditional	0.103±0.042	0.082±0.093	0.141±0.037	0.031±0.023
	Sum Target = 150	0.499±0.002	0.455±0.069	0.500±0.000	0.453±0.117
	Sum Target = 50	0.499±0.002	0.445±0.062	0.500±0.000	0.477±0.031
	Sum Target = 20	0.488±0.005	0.455±0.056	0.500±0.000	0.244±0.100
	Sum Target = -100	0.476±0.015	0.427±0.064	0.500±0.000	0.500±0.000
Predictive Score (Lower is Better)	Unconditional	0.256±0.002	0.065±0.026	0.103±0.002	0.094±0.000
	Sum Target = 150	0.465±0.008	0.146±0.066	0.113±0.001	0.099±0.009
	Sum Target = 50	0.418±0.007	0.107±0.006	0.108±0.001	0.108±0.040
	Sum Target = 20	0.286±0.004	0.104±0.007	0.102±0.001	0.094±0.000
	Sum Target = -100	0.289±0.005	0.106±0.009	0.116±0.003	0.111±0.008
Context-FID Score (Lower is Better)	Unconditional	0.108±0.007	1.230±0.284	0.260±0.024	0.034±0.005
	Sum Target = 150	10.608±1.651	2.648±0.927	2.740±0.480	4.346±0.818
	Sum Target = 50	8.943±1.277	2.408±0.245	2.187±0.115	2.827±0.389
	Sum Target = 20	3.129±0.473	3.533±0.849	0.614±0.111	0.884±0.281
	Sum Target = -100	5.049±0.537	5.056±0.459	3.122±0.389	19.805±1.737
Correlational Score (Lower is Better)	Unconditional	2.313±0.743	0.038±0.013	2.672±0.091	0.066±0.009
	Sum Target = 150	15.328±0.511	0.098±0.010	9.387±0.149	0.297±0.012
	Sum Target = 50	10.872±0.812	0.079±0.015	7.809±0.094	0.210±0.029
	Sum Target = 20	5.219±0.507	0.082±0.011	4.247±0.136	0.111±0.016
	Sum Target = -100	8.345±0.324	0.074±0.002	9.508±0.169	0.837±0.008

D.5. Additional Sum Control Analysis

The following figures provide comprehensive analysis of sum control performance across datasets (Unnormalized). The plots demonstrate achieved sum values compared to target values, with Original and Unconditional (Uncon) baselines as references. Analysis of control weight's impact shows minimal influence on achieved sum values across different datasets and target configurations.

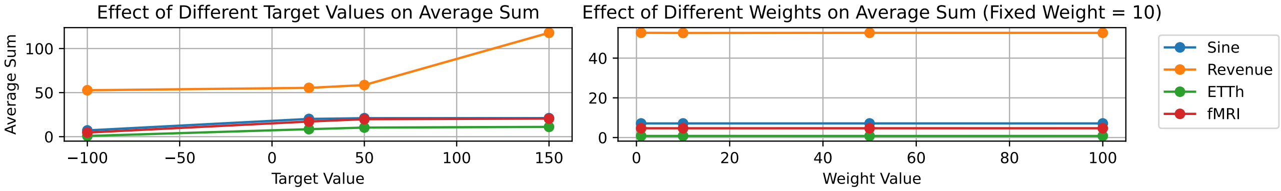

Figure 65. Comparison of achieved sum values versus target sum values across different datasets. The plots demonstrate the effectiveness of sum control guidance in reaching desired targets.

E. Distribution Analysis

The FID scores reveal a fundamental trade-off between controllability and distribution preservation. While Diffusion-TS demonstrates stronger modification capabilities (FID increasing from 0.416 to 16.812 with Anchor control on fMRI), it comes at the cost of significant distribution shifts. In contrast, CSDI shows more resistance to modification but better preserves the original distribution (FID changes from 1.188 to only 1.016 under similar conditions).

This raises an important open question: How can we achieve precise temporal control while maintaining distribution fidelity? Future research should investigate mechanisms to balance these competing objectives, potentially through adaptive control strength or hybrid architectures that combine the stability of CSDI with the flexibility of Diffusion-TS.

Table 11. The complete distribution of discriminative, predictive, correlational, and FID scores for our method across different datasets and control configurations. For all metrics, lower scores indicate better performance.

Model	Metric	Control	ETTh	Revenue	fMRI	Sines
Our - CSDI	Discriminative Score	Unconditional	0.361±0.007	0.245±0.164	0.306±0.021	0.017±0.007
		Anchor Control	0.470±0.003	0.313±0.046	0.482±0.004	0.430±0.038
		Statistics Control	0.373±0.007	0.272±0.055	0.377±0.019	0.034±0.007
	Predictive Score	Unconditional	0.261±0.003	0.054±0.012	0.106±0.000	0.090±0.000
		Anchor Control	0.263±0.001	0.070±0.003	0.106±0.000	0.091±0.000
		Statistics Control	0.261±0.001	0.060±0.005	0.106±0.001	0.091±0.000
	Correlational Score	Unconditional	8.428±0.000	0.034±0.000	2.212±0.000	0.062±0.000
		Anchor Control	8.641±0.000	0.024±0.000	2.619±0.000	0.149±0.000
		Statistics Control	8.531±0.000	0.034±0.000	3.944±0.000	0.065±0.000
	FID Score	Unconditional	1.643±0.171	1.129±0.122	1.188±0.054	0.034±0.006
		Anchor Control	2.720±0.133	2.233±0.088	1.016±0.019	3.170±0.319
		Statistics Control	1.564±0.050	1.097±0.040	1.175±0.018	0.043±0.002
Our - Diffusion-TS	Discriminative Score	Unconditional	0.034±0.026	0.209±0.185	0.089±0.033	0.019±0.008
		Anchor Control	0.437±0.004	0.393±0.030	0.495±0.001	0.460±0.011
		Statistics Control	0.477±0.003	0.426±0.032	0.498±0.001	0.451±0.029
	Predictive Score	Unconditional	0.260±0.002	0.070±0.015	0.110±0.001	0.090±0.000
		Anchor Control	0.314±0.003	0.128±0.011	0.136±0.002	0.153±0.006
		Statistics Control	0.310±0.004	0.114±0.005	0.117±0.001	0.110±0.003
	Correlational Score	Unconditional	1.728±0.000	0.033±0.000	1.673±0.000	0.037±0.000
		Anchor Control	5.647±0.000	0.107±0.000	16.791±0.000	0.405±0.000
		Statistics Control	9.190±0.000	0.083±0.000	8.361±0.000	0.606±0.000
	FID Score	Unconditional	0.177±0.015	1.221±0.040	0.416±0.011	0.021±0.003
		Anchor Control	5.819±0.303	3.479±0.157	16.812±0.485	4.523±0.456
		Statistics Control	5.335±0.221	3.822±0.210	2.652±0.092	5.954±0.438

F. Combined Control on Revenue Dataset

To demonstrate our method's capability to handle multiple control signals simultaneously, we present a comprehensive example using the Revenue dataset. The model successfully generates sequences that respect both anchor points and sum constraints, highlighting the flexibility and effectiveness of our approach. These generated sequences maintain the dataset's inherent distributional characteristics while precisely adhering to multiple control signals. For additional examples of combined control mechanisms, see Figure G which showcases our Time Series Editor interface in action.

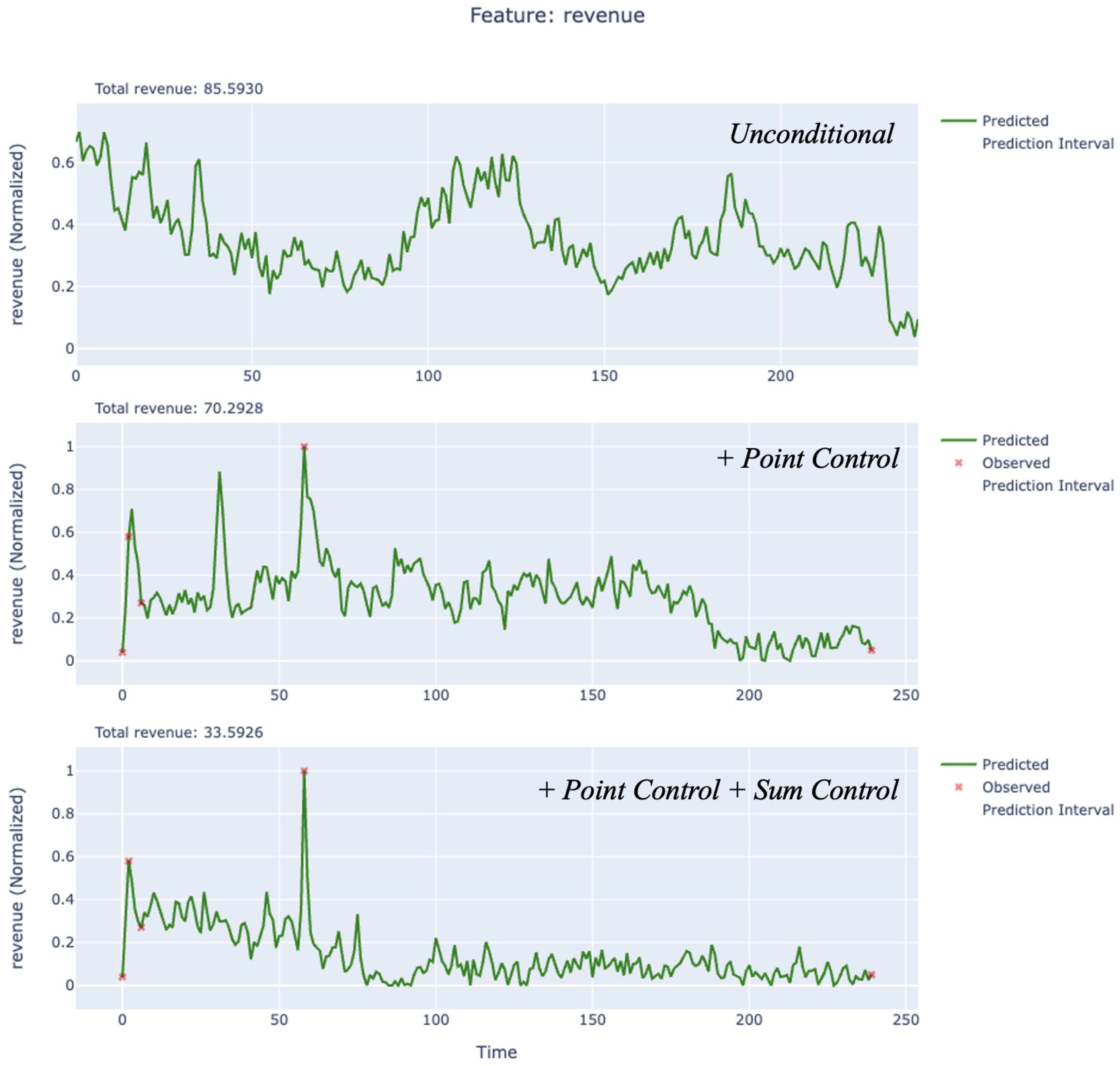

Figure 66. Demonstration of combined anchor and sum control on the Revenue dataset, showing the interaction across point-wise constraints and overall sum requirements.

G. Time Series Editor

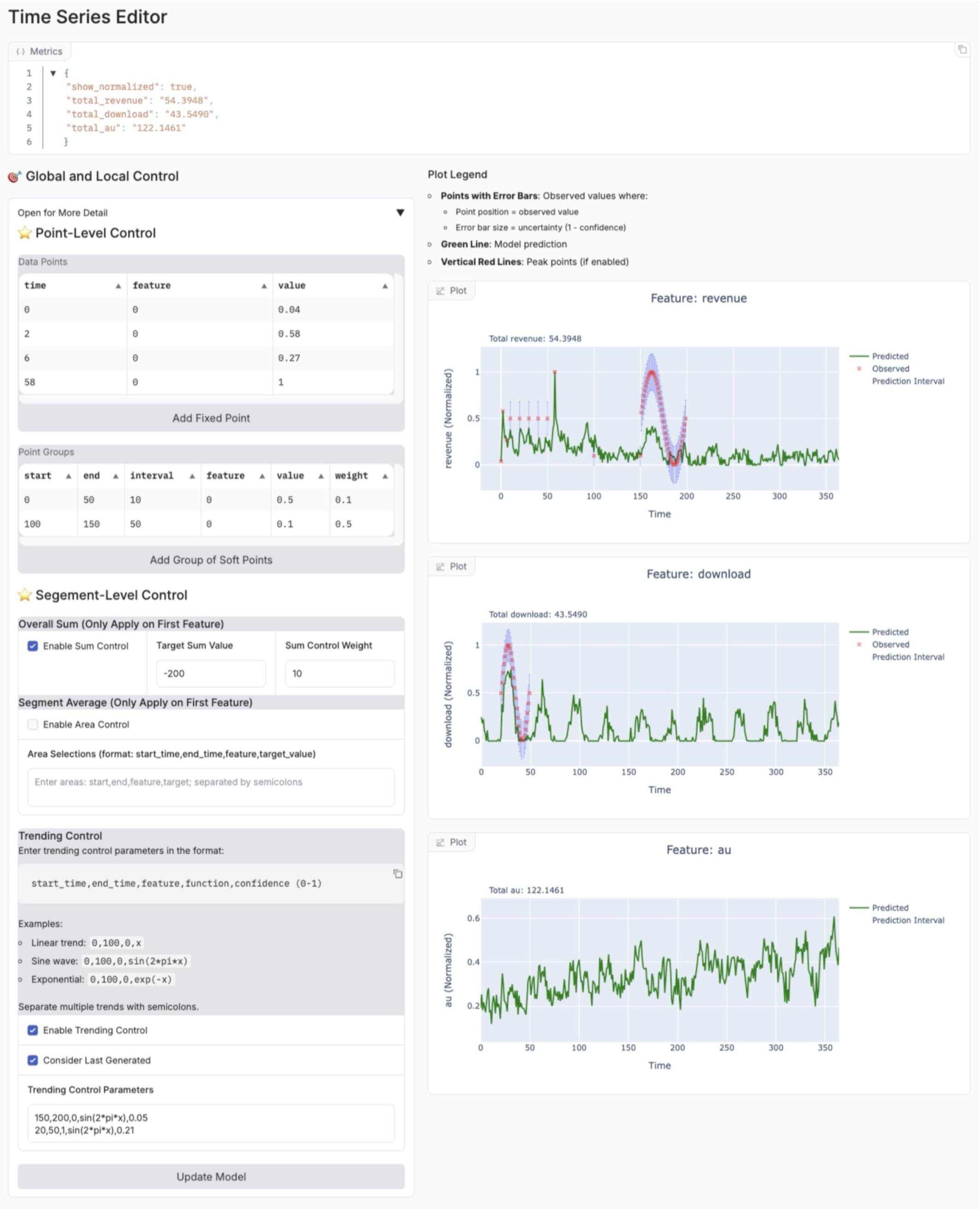

Time Series Editor

Metrics

```
▼ {
  "show_normalized": true,
  "total_revenue": "54.3948",
  "total_download": "43.5490",
  "total_au": "122.1461"
  }
```

Global and Local Control

Open for More Detail ▼

Point-Level Control

Data Points

time	feature	value
0	0	0.04
2	0	0.58
6	0	0.27
58	0	1

Add Fixed Point

Point Groups

start	end	interval	feature	value	weight
0	50	10	0	0.5	0.1
100	150	50	0	0.1	0.5

Add Group of Soft Points

Segement-Level Control

Overall Sum (Only Apply on First Feature)

☑ Enable Sum Control

Target Sum Value: -200

Sum Control Weight: 10

Segment Average (Only Apply on First Feature)

☐ Enable Area Control

Area Selections (format: start_time,end_time,feature,target_value)

Enter areas: start,end,feature,target; separated by semicolons

Trending Control

Enter trending control parameters in the format:

```
start_time,end_time,feature,function,confidence (0-1)
```

Examples:

- Linear trend: `0,100,0,x`
- Sine wave: `0,100,0,sin(2*pi*x)`
- Exponential: `0,100,0,exp(-x)`

Separate multiple trends with semicolons.

☑ Enable Trending Control

☑ Consider Last Generated

Trending Control Parameters

150,200,0,sin(2*pi*x),0.05
20,50,1,sin(2*pi*x),0.21

Update Model

Plot Legend

- **Points with Error Bars**: Observed values where:
  - Point position = observed value
  - Error bar size = uncertainty (1 - confidence)
- **Green Line**: Model prediction
- **Vertical Red Lines**: Peak points (if enabled)

Figure 67. The Screen Shot of Time Series Editor User Interface

The Time Series Editor is designed to solve the Time Series Editing problem. It can add fixed points, soft anchors, trending control, segment-level sum, and average control. For the soft anchors, you can add anchor points based on start, end, and interval setup. The Trending Control is based on the provided function expressions with independent variable x for better precise control. We are currently developing the SketchPad mode for better user interaction, aiming to provide an All-in-One application for efficient time series editing without training.

In Figure G, the green line represents the model prediction, and the red dots represent the observed/provided anchor points. The error bar of each anchor point is the $(1 - \text{confidence})$ to demonstrate the uncertainty of the observed points. In Figure G, we use the Revenue Dataset with three features: Revenue, Download, and Daily Active Users.